Theory of multidimensional parametric band-gap simultons

H. He* and P. D. Drummond
Department of Physics, The University of Queensland, St. Lucia Q4072, Australia
(Received 22 December 1997)

Multidimensional spatiotemporal parametric ''simultons'' (simultaneous solitary waves) are possible in a nonlinear $\chi^{(2)}$ medium with a Bragg grating structure, where large effective dispersion occurs near two resonant band gaps for the carrier and second-harmonic field, respectively. The enhanced dispersion allows much reduced interaction lengths, as compared to bulk medium parametric simultons. The nonlinear parametric band-gap medium permits higher-dimensional stationary waves to form. In addition, solitons can occur with lower input powers than conventional nonlinear Schrödinger equation gap solitons. In this paper, the equations for electromagnetic propagation in a grating structure with a parametric nonlinearity are derived from Maxwell's equation using a coupled mode Hamiltonian analysis in one, two, and three spatial dimensions. Simultaneous solitary wave solutions are proved to exist by reducing the equations to the coupled equations describing a nonlinear parametric waveguide, using the effective-mass approximation (EMA). Exact one-dimensional numerical solutions in agreement with the EMA solutions are also given. Direct numerical simulations show that the solutions have similar types of stability properties to the bulk case, providing the carrier waves are tuned to the two Bragg resonances, and the pulses have a width in frequency space less than the band gap. In summary, these equations describe a physically accessible localized nonlinear wave that is stable in up to $3+1$ dimensions. Possible applications include photonic logic and switching devices. [S1063-651X(98)06109-1]

PACS number(s): 42.65.Tg

I. INTRODUCTION

Parametric ''simultons'' [1–19] (simultaneous solitary waves) have been experimentally observed in $\chi^{(2)}$ media in continuous wave propagation [20], but time-dependent simultons have yet to be generated experimentally. This is due to a number of material requirements, especially that of group-velocity matching, and the necessity of having dispersions of identical sign in both the signal and its harmonic [21]. In addition, nonlinear crystals have a relatively small dispersion. This results in long formation distances, that are easily achieved only in optical fibers (which normally have a $\chi^{(3)}$ rather than a $\chi^{(2)}$ nonlinearity). Despite this, there are clear advantages to the parametric medium for soliton formation. The nonlinear phase shift is much larger at low intensities for parametric nonlinear materials, since it scales as E^2, not E^3. Furthermore, temporal $\chi^{(2)}$ solitary waves are known to exist in more than one spatial dimensions (provided the dispersion is anomalous at both wavelengths) [21]. The bright nonlinear Schrödinger equation (NLS) solitons of a $\chi^{(3)}$ medium are always unstable in higher dimensions.

Bragg grating optical materials have a strong dispersion when the input laser wavelength is nearly equal to twice the refractive index modulation period. Such a strong dispersion has been confirmed experimentally [22]. This makes Bragg gratings an ideal candidate for the formation of $\chi^{(2)}$ simultons with short interaction distances. Using a Bragg grating also helps to solve other problems that occur with conventional parametric solitons. Group-velocity matching is no longer necessary with band gaps: solitons can form even at low or zero velocity in the laboratory frame. In addition, we will show that it is always possible to choose branches of the dispersion relation that give anomalous dispersion at both wavelengths, thus allowing higher-dimensional solitons to form. By comparison, while gap solitons of $\chi^{(3)}$ media are known to occur both experimentally and theoretically [23,24], the formation of these single-wavelength solitons requires very large powers.

We therefore consider combining a $\chi^{(2)}$ nonlinearity with the large dispersion of a band gap, thus creating an ideal spatiotemporal soliton environment [25]. This leads to simultons with a short formation distance and good stability in higher dimensions. The band-gap material can be simply a $\chi^{(2)}$ waveguide with its refractive index periodically modulated, in the case of one-dimensional propagation. Higher-dimensional cases are of the form of planar gratings or layered structures, in two and three spatial dimensions, respectively. In our previous letter [25], we used a Hamiltonian approach to obtain band-gap simultons in one- and two-dimensional cases. In this paper, we give more details of this method, extending it to include treatment of different group velocities, three-dimensional band-gap simultons, and numerical band-gap simulton solutions. The stability of the band-gap simultons is also studied by direct numerical simulations. Band-gap simultons in the one-dimensional case have also recently been considered in two related papers, using numerical techniques [26] and a multiscaling method [27].

II. PARAMETRIC GAP EQUATION

In this section, a one-dimensional parametric gap equation is derived from the Maxwell equations. We assume that the medium is isotropic. A more comprehensive tensor theory would include the treatment of birefringent crystals, which

*Present address: Department of Theoretical Physics, School of Physics A28, The University of Sydney, Sydney 2006, Australia.

can allow phase matching between the fundamental and the second harmonic, even in the presence of material dispersion. We omit this effect in the interest of simplicity. The one-dimensional equation can also be generalized to higher-dimensional equations including diffraction. We will treat this important case in Sec. III, which gives a rigorous treatment of the three-dimensional problem including the effects of wave-guiding structures.

One-dimensional Maxwell equations

The one-dimensional Maxwell equation describing the propagation of a linear polarized electric field **E** and displacement field **D** can be written as

$$\frac{\partial^2 \mathbf{E}}{\partial z^2} = \mu_0 \frac{\partial^2 \mathbf{D}}{\partial t^2}, \tag{2.1}$$

where μ_0 is the vacuum permeability, and **D** and **E** are perpendicular to the propagation direction z. The displacement field **D** is

$$\mathbf{D} = \epsilon_0 \mathbf{E} + \mathbf{P}_L + \mathbf{P}_{\mathrm{NL}}, \tag{2.2}$$

where the linear polarization is given by a causal response function

$$\mathbf{P}_L = \epsilon_0 \int_{-\infty}^{\infty} \chi^{(1)}(z, t-\tau)\mathbf{E}(z,\tau)\, d\tau, \tag{2.3}$$

and the nonlinear polarization is given in the Bloembergen expansion by

$$\mathbf{P}_{\mathrm{NL}} \approx \epsilon_0 \chi^{(2)} : \mathbf{E}\mathbf{E} + \cdots. \tag{2.4}$$

The first order susceptibility $\chi^{(1)}$ is a second-rank tensor, and the quadratic susceptibility $\chi^{(2)}$ is a third-rank tensor in general. However, we will not treat this general situation in detail. For simplicity, we suppose that $\chi^{(1)}$ is rotationally symmetric, which means that we will consider only its scalar form. In this paper, we consider second order nonlinearity, and therefore include only up to second order susceptibility in the nonlinear polarization. We also assume that $\chi^{(2)}$ dispersion is small enough to be neglected here.

For a quasimonochromatic electric field in a second-harmonic generation process, we can write the solutions to the Maxwell's equation for frequencies near ω_1, ω_2 as

$$\mathbf{E} = \sum_{j=1,2} \sum_{\pm} \mathbf{e}_j \mathcal{A}_{j\pm}(z,t) e^{\pm i j\bar{k} z - i\omega_j t} + \text{c.c.}, \tag{2.5}$$

where $\mathbf{e}_j$ are the polarizations, $\omega_2 = 2\omega_1$, the sign $p = \pm$ represents right or left propagation, and $j\bar{k}$ is the effective wave vector of the corresponding carrier field. It is important to note that the actual wave number of the propagating fields can differ from $j\bar{k}$, since the envelope function can vary in space; thus $\bar{k}$ is simply chosen as close to the relevant wave numbers. In this paper, it actually corresponds to the refractive-index modulation wave number.

We therefore can write $\mathbf{P}_L$ as

$$\mathbf{P}_L = \epsilon_0 \sum_j \sum_{\pm} \int_{-\infty}^{\infty} \chi^{(1)}(z,\tau)\mathbf{e}_j \mathcal{A}_{j\pm} \times (z, t-\tau) e^{\pm i j\bar{k} z - i\omega_j (t-\tau)} d\tau + \text{c.c.} \tag{2.6}$$

Transforming $\mathcal{A}_{j\pm}$ into frequency space and defining

$$\tilde{\chi}^{(1)}(z, \omega+\omega_j) = \int_{-\infty}^{\infty} \chi^{(1)}(z,\tau) e^{i(\omega+\omega_j)\tau} d\tau, \tag{2.7}$$

we have

$$\mathbf{P}_L = \epsilon_0 \sum_j \sum_{\pm} \int_{-\infty}^{\infty} \mathbf{e}_j \tilde{\chi}^{(1)} \times (z, \omega+\omega_j) \mathcal{A}_{j\pm}(z,\omega) e^{\pm i j\bar{k} z - i(\omega+\omega_j)t} d\omega + \text{c.c.} \tag{2.8}$$

Expanding $\tilde{\chi}^{(1)}(\omega+\omega_j)$ around ω_j into a power series up to first order in ω, we find that

$$\mathbf{D} = \sum_j \sum_{\pm} \mathbf{e}_j \left(\epsilon_j(z) \mathcal{A}_{j\pm}(z,t) + i\epsilon_j'(z) \frac{\partial \mathcal{A}_{j\pm}(z,t)}{\partial t} \right) \times e^{\pm i j\bar{k} z - i\omega_j t} + \mathbf{P}_{\mathrm{NL}} + \text{c.c.}, \tag{2.9}$$

where $\epsilon_j(z) = \epsilon_0[1 + \tilde{\chi}^{(1)}(z,\omega_j)]$ and $\epsilon_j'(z) = \epsilon_0 \partial \tilde{\chi}^{(1)}(z,\omega)/\partial\omega|_{\omega j}$ are the permittivities and their derivatives at the fundamental and second-harmonic frequencies.

The spatial variation of $\chi^{(1)}$ is chosen to correspond to a Bragg grating structure with $\epsilon_j(z) = \bar{\epsilon}_j[1 + \Delta_j(z)]$, where $\bar{\epsilon}_j$ is the spatial average of $\epsilon_j(z)$, and $j = 1$ and 2. In general, we will consider $\Delta_j(z)$ to be a small parameter here, and the results will be expanded in terms of a small parameter $\Delta > \Delta_j(z)$. This notation also allows us to distinguish the spatial modulation present at frequency ω_1 from the (generally different) spatial modulation present at frequency ω_2. Each carrier wave at these distinct frequencies will experience a rather complex modulated refractive index. However, the resonant properties of Bragg gratings means that each will only interact strongly with a Fourier component having half the respective carrier wavelength. Here the permittivity $\epsilon_j(z)$ is a periodic function with period d. We can expand $\epsilon_j(z)$ in a Fourier series, with

$$\Delta_j(z) = \sum_l \Delta_{jl} \exp(2il\bar{k}z) + \text{c.c.}, \tag{2.10}$$

given that Δ_{jl} are complex coefficients, and $\bar{k} = \pi/d = 2\pi\bar{n}_1/\lambda_1$, where λ_1 is the free-space wavelength of the fundamental field. The refractive index at the first carrier frequency is given by $\bar{n}_1 = \sqrt{\bar{\epsilon}_1/\epsilon_0}$. More general types of grating can be treated, but this is sufficient to treat the gap soliton. For reference purposes later, we note that if Δ_{jl} is real and positive, the refractive index has a $\cos(2l\bar{k}z)$ modulation, with a maximum in the refractive index occurring at the origin.

The conceptually simplest grating is that the modulation of refractive index is the superposition of two sinusoidal

waves—only terms with Δ_{j1} and Δ_{j2} in Eq. (2.10) exist. It is possible that the two coefficients are of opposite signs, and the two modulations are then out of phase. It is highly desirable that band gaps occur at both the carrier wavelengths, in order to optimize the nonlinear coupling between the waves. This is because the resonant modes of the linear Maxwell equations near a band gap are quasistanding waves—and these will only couple strongly to other standing waves.

A more practical modulation of the refractive index is of a nearly square-wave shape. One can fabricate this grating by using laser interference patterns in a saturated photosensitive material, thus giving rise to higher order harmonics. This type of grating is also capable of supporting band gaps at higher harmonics of the optical carrier frequency. Thus it is possible in principle to have strongly coupled simultons of more complex types, by considering appropriately engineered Bragg gratings with several distinct spatial frequencies. An obvious example of this would be a nondegenerate parametric simulton requiring three distinct spatial frequencies defined so that $k_1+k_2=k_3$.

We define $k_j=k(\omega_j)=\sqrt{\mu_0\bar{\epsilon}_j}\omega_j$ as the linear wave number, $\delta k_j=k_j-j\bar{k}\ll j\bar{k}$, and substitute Eqs. (2.9) and (2.10) into the Maxwell equation (2.1). Neglecting terms with third order differentiation, we arrive at

$$\sum_{j=1}^{2}\mathbf{e}_j\Bigg\{\Bigg[2ij\bar{k}\frac{\partial\mathcal{A}_{j+}}{\partial z}+\frac{\partial^2\mathcal{A}_{j+}}{\partial z^2}+\mu_0\bar{\epsilon}_j\Delta_{jj}\omega_j^2\mathcal{A}_{j-}+[\mu_0\bar{\epsilon}_j\omega_j^2-(k_j-\delta k_j)^2]\mathcal{A}_{j+}+i\frac{2k_j}{v_j}\frac{\partial\mathcal{A}_{j+}}{\partial t}-(\epsilon_j+2\omega_j\epsilon_j')\frac{\partial^2\mathcal{A}_{j+}}{\partial t^2}\Bigg]e^{-ij(\omega_1 t-k_1)z}+\Bigg[-2ij\bar{k}\frac{\partial\mathcal{A}_{j-}}{\partial z}+\frac{\partial^2\mathcal{A}_{j-}}{\partial z^2}+\mu_0\bar{\epsilon}_j\Delta_{jj}j^2\omega_1^2\mathcal{A}_{j+}+[\mu_0\bar{\epsilon}_j\omega_j^2-(k_j-\delta k_j)^2]\mathcal{A}_{j-}+i\frac{2k_j}{v_j}\frac{\partial\mathcal{A}_{j-}}{\partial t}-\mu_0(\epsilon_j+2\omega_j\epsilon_j')\frac{\partial^2\mathcal{A}_{j-}}{\partial t^2}\Bigg]e^{-ij(\omega_1 t+k_1)z}\Bigg\}=\mu_0\frac{\partial^2\mathbf{P}_{\mathrm{NL}}}{\partial t^2},\quad(2.11)$$

where $v_j=d\omega/dk|_{\omega j}=\omega_j/[k_j(1+\omega_j\epsilon_j'/(2\epsilon_j))]$.

Assuming that $\mathcal{A}_j$ are slowly evolving, we neglect group velocity dispersion terms involving $\partial^2/\partial t^2$ and $\partial^2/\partial z^2$. Terms involving δk_j^2 or first order differentiation and δk_j are also neglected, for they are much smaller than these terms involving only δk_j or first order differentiation, which we call first order terms. Retaining only the first order phase-matched terms of the above equation, we have

$$i\left[\frac{1}{v_1}\frac{\partial}{\partial t}+\frac{\partial}{\partial z}\right]\mathcal{A}_{1+}+\delta k_1\mathcal{A}_{1+}+\kappa_1\mathcal{A}_{1-}+\chi_E\mathcal{A}_{1+}^*\mathcal{A}_{2+}=0,$$

$$i\left[\frac{1}{v_1}\frac{\partial}{\partial t}-\frac{\partial}{\partial z}\right]\mathcal{A}_{1-}+\delta k_1\mathcal{A}_{1-}+\kappa_1^*\mathcal{A}_{1+}+\chi_E\mathcal{A}_{1-}^*\mathcal{A}_{2-}=0,$$

$$i\left[\frac{1}{v_2}\frac{\partial}{\partial t}+\frac{\partial}{\partial z}\right]\mathcal{A}_{2+}+\delta k_2\mathcal{A}_{2+}+\kappa_2\mathcal{A}_{2-}+\chi_E\mathcal{A}_{1+}^2=0,$$

$$i\left[\frac{1}{v_2}\frac{\partial}{\partial t}-\frac{\partial}{\partial z}\right]\mathcal{A}_{2-}+\delta k_2\mathcal{A}_{2-}+\kappa_2^*\mathcal{A}_{2+}+\chi_E\mathcal{A}_{1-}^2=0,\quad(2.12)$$

where

$$\chi_E=\omega_1^2\tilde{\chi}^{(2)}/(\bar{k}c^2),$$

$$\tilde{\chi}^{(2)}=\mathbf{e}_1^*\cdot\chi^{(2)}\cdot\mathbf{e}_1^*\mathbf{e}_2=\mathbf{e}_2^*\cdot\chi^{(2)}\cdot\mathbf{e}_1\mathbf{e}_1,\ \text{and}\ \kappa_j=j\bar{k}\Delta_{jj}/2.$$

To simplify the equations, we can always choose the phases of $\mathbf{e}_j$ so that χ_E is real. We neglect the group-velocity dispersion of the medium, as this is usually much smaller than the gap dispersion. However, we have included the difference in group velocity between the two carriers, as this is not always negligible.

III. BAND GAP IN ONE DIMENSION

Without the grating structure, the dispersion relation (frequency ω versus wave number k) would be a continuous straight line in the vicinity of the gap frequency. Introducing a grating structure opens a gap at the edge of the Brillouin zone for each of the carrier frequencies. Inside each gap, light is completely Bragg reflected, resulting in strong dispersion near the critical gap frequencies. The eigenmodes of the Maxwell equations in the vicinity of the gap are also modified. Instead of the usual plane waves, the eigenmodes become modulated quasistanding waves, with a pure standing wave being achieved exactly at the wave number for resonance. In this case there are two possible standing wave solutions with different spatial phases [i.e., $\sin(\bar{k}z)$ and $\cos(\bar{k}z)$ solutions]. These are familiar in electronic band-gap theory, and have the usual property that one has an eigenfrequency above, and the other below, the gap center frequency. Propagation of a free field with a frequency in the gap region is, of course, prohibited. However, in the presence of the nonlinear medium, it is possible that propagation can occur due to nonlinear phase shifts.

One-dimensional dispersion relation

The dispersion relation of the one-dimensional Maxwell equations in the slowly-varying envelope approximation can be obtained by studying the linear part of the gap parametric equations (2.12). Neglecting the nonlinear terms, we have the linear coupled equations

$$i\left[\frac{1}{v_j}\frac{\partial}{\partial t}+\frac{\partial}{\partial z}\right]\mathcal{A}_{j+}+\delta k_j\mathcal{A}_{j+}+\kappa_j\mathcal{A}_{j-}=0,$$

$$i\left[\frac{1}{v_j}\frac{\partial}{\partial t}-\frac{\partial}{\partial z}\right]\mathcal{A}_{j-}+\delta k_j\mathcal{A}_{j-}+\kappa_j^*\mathcal{A}_{j+}=0.\quad(3.1)$$

Following standard techniques [24], we introduce a vector for the right and left propagating fields:

$$\vec{\mathcal{A}}_j(z,t)=\begin{bmatrix}\mathcal{A}_{j+}\\ \mathcal{A}_{j-}\end{bmatrix}. \tag{3.2}$$

Inserting the ansatz

$$\vec{\mathcal{A}}_j(z,t)=\vec{f}_j(Q)e^{i(Qz-\Omega_j t)},\quad j=1,2, \tag{3.3}$$

into the linear equation (3.1), one obtains the algebraic equation

$$\begin{bmatrix}\Omega_j/v_j-Q+\delta k_j & \kappa_j\\ \kappa_j^* & \Omega_j/v_j+Q+\delta k_j\end{bmatrix}\begin{bmatrix}f_{j+}\\ f_{j-}\end{bmatrix}=0. \tag{3.4}$$

Solving the above equation for Q, we have two eigenvalues corresponding to $s=\pm 1$,

$$\Omega_j^{(s)}(Q)=v_j(s\sqrt{Q^2+|\kappa_j^2|}-\delta k_j),\quad j=1,2. \tag{3.5}$$

If $\delta k_j=0$, this equation becomes the dispersion relationship found in conventional $\chi^{(3)}$ band-gap systems [24]. The width of each band gap in the dispersion relation is then given by

$$\Delta\Omega_j=\Omega_j^+(0)-\Omega_j^-(0)=2v_j|\kappa_j|. \tag{3.6}$$

Substituting the above solutions [Eq. (3.5)] into the linear equation, we obtain two sets of normalized eigenvectors, corresponding to linear propagation above and below the band gap:

$$\vec{f}_j^{(s)}(Q)=\frac{[\kappa_j,Q-s\sqrt{|\kappa_j^2|+Q^2}]^T}{\sqrt{2(|\kappa_j^2|+Q^2-sQ\sqrt{|\kappa_j^2|+Q^2})}}, \tag{3.7}$$

where the sign $s=-1$ corresponds to the lower branch, and $s=1$ to the upper branch.

The physical meaning of the s parameter is clearest in the case of $Q=0$, which is in the center of the band gap in k space. Suppose, for simplicity, that the jth refractive index has a local maximum at $z=0$. This corresponds to a $\cos(2\overline{kj}z)$ modulation of the refractive index, so that $\kappa_j>0$. In general, we can always choose the origin so that this is true for at least one of the carrier frequencies, although it might not be true for both. In this case the lower branch ($s=-1$) also has a symmetric form, with a $\cos(\overline{kj}z)$ modulation. The upper branch has an antisymmetric $\sin(\overline{kj}z)$ mode function. We can understand this physically if we argue that a lower energy—and hence a lower frequency—is obtained when the maximum field intensity in space corresponds to the maximum refractive index in space, which means the maximum dielectric polarization. In Sec. IV, we see that this is justified by the Hamiltonian theory of the dielectric plus radiation system.

The dispersion relation [Eq. (3.5)] is depicted in Fig. 1 for one of the band gaps. Because of the gap, linear propagation is not allowed if the frequency shift from the gap center is small, i.e., $|\Omega|<v_j|\kappa_j|$. This results in strong dispersion, so that

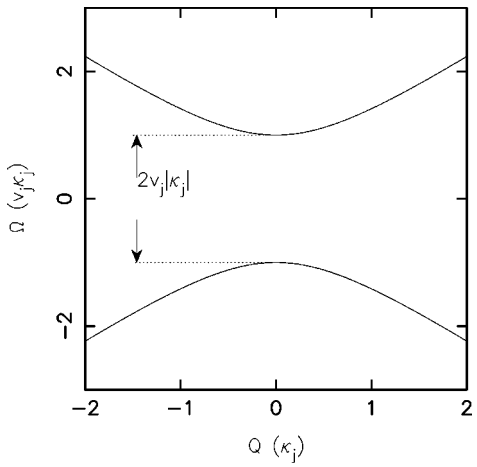

FIG. 1. Dispersion relation for light with wave numbers around $k_j=j\pi/d$, where d is the period of the grating. The width of the gap is given as $\Delta\Omega=\Omega^+-\Omega^-=2v_j|\kappa_j|$. For simplicity, Ω is plotted with a unit of $v_j\kappa_j$, while Q is plotted with a unit of κ_j.

$$\frac{d^2\Omega_{js}}{dQ^2}=\frac{sv_j|\kappa_j^2|}{(Q^2+|\kappa_j^2|)^{3/2}}. \tag{3.8}$$

The dispersion ($\omega''=d^2\omega/dk^2$) of typical nonlinear optical media is of the order of 10^{-1} m^2/s at a wavelength of 1 μm. In the case of lithium niobate, the corresponding refractive index is $\overline{n}\simeq 2.5$. Assuming 0.2% refractive index modulation, so that $\Delta_{jj}=0.002$, we find that κ_j is of the order of 10^4 m^{-1}. This indicates a maximum band-gap dispersion of $v_j/|\kappa_j|\simeq 10^4$ m^2/s. Such a strong dispersion gives an advantage in reducing soliton formation length significantly, and has been recently confirmed experimentally [22]. The large gap-induced dispersion provides a justification for our neglect of material group-velocity dispersion effects in these equations.

IV. HAMILTONIAN METHOD

Traditionally, there are two approaches to solving soliton equations. The first is the inverse scattering method, which gives a complete exact analytic solutions for NLS-type equations. This method has not yet been applied to parametric equations. In fact, these equations appear to be generically nonintegrable. Another approach is the virtual particle method, which treats soliton formation as equivalent to the equation of motion of a virtual particle in a nonlinear field [28,16]. A soliton solution in this picture corresponds to a path that connects two critical points (topological soliton) or an enclosed path that passes one critical point (nontopological soliton), where a critical point is a point at which the virtual particle experiences no ''force'' from the nonlinear field. This picture gives a clear physical understanding of soliton equations. Based on the topological nature of the nonlinear field, we can thus classify soliton solutions. The difficulty of this method is to find the soliton paths—which may not be represented analytically, but can be expressed numerically. Such a task is relatively easy if the nonlinear field has a low dimension.

This topological method has been applied successfully to the parametric equations including dispersion [16]. Without

actually solving the equations, the method treats them as a pair of Newtonian equations describing the motion of a virtual particle in a two-dimensional acceleration field. The existence and parameter ranges can be obtained by studying the topological structure of the acceleration field. Based on the information from these analyses, numerical solutions can then be obtained easily. The nonlinear field of the parametric gap equation is at least four dimensional (in phase space), and identifying a soliton path involves at least three free parameters. In applying this method to the parametric gap equations, it is simpler to reduce them into two nonlinear coupled second order equations. In order to achieve this simplification, we next turn to approximate Hamiltonian techniques for analyzing the gap soliton. In a later section, the physical insight obtained from this approach will allow us to find a large family of solutions to the full set of equations, using acceleration field arguments—together with numerical solutions of the virtual particle equations.

A. Hamiltonian

We will show that by using a Hamiltonian method for propagation near the center of the band gap, an approximate pair of coupled second order equations can be derived. This allows a topological classification of the grating solitons, using previously known techniques. The Hamiltonian theory also permits us to describe waveguide mode structures in a very simple way. We note that the Hamiltonian for a nonlinear medium is most readily written using the displacement field as a canonical variable, as pointed out by Hillery and Mlodinow [29]. When using the displacement field as the canonical variable, it is most natural to expand the electric field in a formal power series in the displacement field, using inverse permittivity tensors as expansion coefficients. Thus, in the absence of dispersion

$$E_i(t,\mathbf{x})=\sum_{jn}\ \eta^{(n)}_{i,i_1\ldots i_{jn}}(\mathbf{x})D_{i1}(t,\mathbf{x})\ \ldots D_{i_{jn}}(t,\mathbf{x}). \tag{4.1}$$

Extending the above expansion to include linear dispersion, the complete Hamiltonian [30,31] can be written as

$$H=H_0+H_{\rm int}, \tag{4.2}$$

where the linear and nonlinear terms are, respectively,

$$H_0=\int\ \sum_j\ \left(\frac{1}{\mu_0}|\vec{\mathcal{B}}_j|^2+\eta(\mathbf{x},\omega_j)^2\frac{\partial}{\partial\omega_j}\left[\frac{\omega_j}{\eta(\mathbf{x},\omega_j)}\right]\vec{\mathcal{D}}_j^*\vec{\mathcal{D}}_j\right)d^3\mathbf{x},$$

$$H_{\rm int}=\tfrac{1}{3}\int\ \mathbf{D}\cdot\ \eta^{(2)}:\mathbf{DD}\ d^3\mathbf{x}. \tag{4.3}$$

Here $\mathbf{x}=(\mathbf{r},z)$, while $\mathbf{r}=(x,y)$ are the transverse coordinates and z is the longitudinal coordinate. We have introduced an inverse permittivity, $\eta(\mathbf{x},\omega)=1/[\,\epsilon(\mathbf{x},\omega)\,]$ for convenience. Similar to ϵ, we assume η to be rotational symmetric and only consider its scalar form here. We also define $\eta^{(2)}=-\epsilon_0\chi^{(2)}/(\epsilon_1^2\epsilon_2)$ [29], $\mathbf{D}=\Sigma_{j=1,2}(\vec{\mathcal{D}}_j+\vec{\mathcal{D}}_j^*)$, and $\mathbf{B}=\Sigma_{j=1,2}(\vec{\mathcal{B}}_j+\vec{\mathcal{B}}_j^*)$. In Sec. III, the electric field is expressed as a pair of antipropagating waves based on the coupled mode theory. Here we start from the most general form of these fields in a three-dimensional medium.

We emphasize that this approach is capable of generating the full Maxwell's equations in four dimensions. The Hamiltonian clearly separates into a linear part and a nonlinear part. We first start with the linear part. This will allow us to identify mode structures, which leads to some useful approximations later.

B. Linear part of the Hamiltonian and mode expansion

Our objective in this section is to calculate the linear mode expansion of the wave equation in a three-dimensional medium that includes a weak refractive index modulation in the z direction. We also consider cases in which there is a transverse variation of the refractive index, causing either a one- or two-dimensional waveguide to occur. The calculation of the mode structure will be carried out to first order in the refractive index modulation. In all cases we are primarily interested in volume gratings that extend throughout the region of interest; that is, the grating is quasihomogeneous. It is also possible to fabricate inhomogeneous gratings—for example, by surface modulation of a two-dimensional waveguide. We do not consider this case here, and our results are not applicable to surface gratings.

Although we only intend to obtain classical equations, it is convenient to follow the normalization of the standard quantization procedure [30,32,33]. We introduce the dual potential $\mathbf{\Lambda}$ [29], defined so that $\vec{\mathcal{D}}=\nabla\times\mathbf{\Lambda}$ and $\vec{\mathcal{B}}=\mu\partial_t\mathbf{\Lambda}$, which is useful for obtaining a nonlinear Hamiltonian theory. We express $\mathbf{\Lambda}$ in terms of mode functions $\mathbf{\Lambda_{jn}}$ normalized over a length L. Periodic boundary conditions are imposed at $x_i=0,x_i=L$, where $x_i=x,y,z$, and we later take $L\to\infty$. The mode expansion is taken to be

$$\mathbf{\Lambda}(t,\mathbf{x})=\frac{1}{\sqrt{L}}\sum_{\mathbf{jn}}\ a_{j\mathbf{n}}(t)\mathbf{\Lambda_{jn}}(\mathbf{x}). \tag{4.4}$$

Here $a_{j\mathbf{n}}\propto e^{-i\omega_{j\mathbf{n}}t}$, and $\mathbf{n}$ refers to all mode indices. We choose $\mathbf{\Lambda}_{j\mathbf{n}}$ to be transverse.

Hence we can write

$$\vec{\mathcal{D}}=\frac{1}{\sqrt{L}}\sum_{\mathbf{jn}}\ \nabla\times\mathbf{\Lambda}_{j\mathbf{n}}a_{j\mathbf{n}},$$

$$\vec{\mathcal{B}}=\frac{-i}{\sqrt{L}}\sum_{\mathbf{jn}}\ \mu_0\omega_{j\mathbf{n}}\mathbf{\Lambda}_{j\mathbf{n}}a_{j\mathbf{n}}. \tag{4.5}$$

With this definition, the positive frequency part of the electric field ($\vec{\mathcal{E}}$) can be written as $\vec{\mathcal{E}}(\mathbf{x},\omega)=\eta(\mathbf{x},\omega)\vec{\mathcal{D}}(\mathbf{x},\omega)-\vec{\mathcal{P}}_{NL}(\mathbf{x},\omega)/\epsilon_0$. However, for evaluating mode functions, we temporarily consider just the linear Maxwell equations. Substituting the above expansion into the Maxwell equation $\nabla\times\vec{\mathcal{E}}=-\partial_t\vec{\mathcal{B}}$ gives a wave equation, and hence an eigenvalue equation for mode functions $\mathbf{\Lambda}_{j\mathbf{n}}$ with eigenvalues $\omega_{j\mathbf{n}}$, as follows:

$$\nabla\times[\,\eta(\mathbf{x},\omega_{j\mathbf{n}})\nabla\times\mathbf{\Lambda}_{j\mathbf{n}}]=\mu\omega_{j\mathbf{n}}^2\mathbf{\Lambda_{jn}}. \tag{4.6}$$

Expanding $\vec{\mathcal{D}}$ and $\vec{\mathcal{B}}$ in terms of modes that satisfy the above equation in the linear part of the Hamiltonian gives the result

$$H_L=\sum_{j\mathbf{n}}\hbar\omega_{j\mathbf{n}}a^*_{j\mathbf{n}}a_{j\mathbf{n}}. \tag{4.7}$$

In order to use this result, we need to develop approximate expressions for the mode eigenvalues and eigenfunctions, in the typical case of weakly guided waves in one and two dimensions, as well as a full three-dimensional bulk crystal layered structure. In a weakly guided waveguide, we assume that that the permittivity factorizes into longitudinally and transversely varying parts, so that

$$\epsilon(\mathbf{x},\omega)=\tilde{\epsilon}(z,\omega)\epsilon_r(\mathbf{r})=1/\eta(\mathbf{x},\omega), \tag{4.8}$$

where, in the vicinity of the jth carrier frequency, $\epsilon_r(\mathbf{r})=1+\Delta_{jr}(\mathbf{r})=1/\eta_r(\mathbf{r})$, $\tilde{\epsilon}(z,\omega)=\overline{\epsilon}(\omega)[1+\Delta_j(z)]=1/\tilde{\eta}(z,\omega)$, and $\overline{\eta}(\omega)=1/\overline{\epsilon}(\omega)$. Both $\Delta_{jr}(\mathbf{r})$ and $\Delta_j(z)$ are small quantities. The inverse permittivity is given to first order by

$$\eta(\mathbf{x},\omega)\approx\overline{\eta}(\omega)[1-\Delta_{jr}(\mathbf{r})-\Delta_j(z)]. \tag{4.9}$$

We also assume that the transverse permittivity varies much slower than the longitudinal permittivity, as is usually the case for weakly guided waves with a modal dimension much greater than a wavelength. This means that we have $\nabla\eta\approx\nabla\tilde{\eta}$.

Next, suppose that $\mathbf{n}=(\mathbf{m},n)$, and each spatial mode is approximately factorizable into the form

$$\mathbf{\Lambda}_{j\mathbf{n}}=\mathbf{\Lambda}_{jn}(\mathbf{r},z)=\mathbf{u}_{j\mathbf{m}}(\mathbf{r})\Lambda_{jn}(z), \tag{4.10}$$

where the direction of the $\mathbf{\Lambda}_{jn}(\mathbf{x},z)$ totally depends on $\mathbf{u}_{j\mathbf{m}}(\mathbf{r})$, and $\nabla\Lambda_{jn}\cdot\mathbf{u}_{j\mathbf{m}}\approx 0$. Since $\nabla\cdot\mathbf{\Lambda}=0$, we have $\nabla\cdot(\Lambda_{jn}\mathbf{u}_{j\mathbf{m}})=0$, which gives $\nabla\cdot\mathbf{u}_{j\mathbf{m}}\approx 0$.

Substituting the above two expressions into the eigenvalue equation (4.6), we obtain

$$\nabla\eta\times[\nabla\times(\Lambda_{jn}\mathbf{u}_{j\mathbf{m}})]+\eta\nabla\times[\nabla\times(\Lambda_{jn}\mathbf{u}_{j\mathbf{m}})]=\mu_0\omega^2_{j\mathbf{n}}\Lambda_{jn}\mathbf{u}_{j\mathbf{m}}. \tag{4.11}$$

To simplify the above equation, we work out the following relationships, with the permittivities are all evaluated at the eigenfrequency $\omega_{j\mathbf{n}}$:

$$\nabla\times[\nabla\times(\Lambda_{jn}\mathbf{u}_{j\mathbf{m}})]\approx-\frac{\partial^2\Lambda_{jn}}{\partial z^2}\mathbf{u}_{j\mathbf{m}}-\Lambda_{jn}\nabla_r^2\mathbf{u}_{j\mathbf{m}},$$

$$\nabla\eta\times[\nabla\times(\Lambda_{jn}\mathbf{u}_{j\mathbf{m}})]\approx-\eta_r\frac{\partial\tilde{\eta}}{\partial z}\frac{\partial\Lambda_{jn}}{\partial z}\mathbf{u}_{j\mathbf{m}}, \tag{4.12}$$

where $\nabla_r^2=\partial^2/\partial x^2+\partial^2/\partial y^2$, and the conditions $\nabla\cdot\mathbf{u}_{j\mathbf{m}}=0$ and $\nabla\Delta_{jr}\approx 0$ have been used, together with the relation that $\nabla\Lambda_{jn}\times(\nabla\times\mathbf{u}_{j\mathbf{m}})=0$.

Dividing both sides of the equation by η, and retaining terms up to first order in Δ_{jr} and Δ_j we arrive at

$$\left(\frac{\partial\Delta_j}{\partial z}\frac{\partial\Lambda_{jn}}{\partial z}-\frac{\partial^2\Lambda_{jn}}{\partial z^2}\right)\mathbf{u}_{j\mathbf{m}}-\nabla_r^2\mathbf{u}_{j\mathbf{m}}\Lambda_{jn}=\frac{\mu_0\omega^2_{j\mathbf{n}}}{\eta(\mathbf{x},\omega_{j\mathbf{n}})}\Lambda_{jn}\mathbf{u}_{j\mathbf{m}}. \tag{4.13}$$

To simplify the right-hand side of the above equation, we now expand the eigenfrequencies near the jth carrier frequency of interest, as $\omega_{j\mathbf{n}}=\omega_j+\Delta\omega_{j\mathbf{m}}+\Omega_{jn}$, where $\Delta\omega_{j\mathbf{m}}$ and Ω_{jn} are small quantities when compared with ω_j. We next expand the permittivity around ω_j to first order, thus including group-velocity effects in the material dispersion. This gives

$$\mu_0\frac{\omega^2_{j\mathbf{n}}}{\eta(\mathbf{x},\omega_{j\mathbf{n}})}\approx k_j^2[1+\Delta_j(z)+\Delta_{jr}(\mathbf{r})]+2[\Delta\omega_{j\mathbf{m}}+\Omega_{jn}]k_j/v_j. \tag{4.14}$$

Introducing $\tilde{\omega}_{jn}=\omega_j[1+\Omega_{jn}/(k_jv_j)]$, the eigenvalue equation hence becomes separable, with group-velocity effects included. There is one transverse mode equation, and one longitudinal mode equation for $\mathbf{u}_{j\mathbf{n}}$ and Λ_{jn}, to first order in Δ:

$$[\nabla_r^2+k_j^2\Delta_{jr}(\mathbf{r})]\mathbf{u}_{j\mathbf{m}}(\mathbf{r})=-2(k_j/v_j)\Delta\omega_{j\mathbf{m}}\mathbf{u}_{j\mathbf{m}}(\mathbf{r}),$$
$$\left[\tilde{\eta}_j(z)\frac{\partial^2}{\partial z^2}+\frac{\partial\tilde{\eta}_j(z)}{\partial z}\frac{\partial}{\partial z}\right]\Lambda_{jn}(z)=-\mu_0\tilde{\omega}^2_{jn}\Lambda_{jn}(z). \tag{4.15}$$

Here $\tilde{\eta}_j(z)=\tilde{\eta}(z,\omega_j)$ is just the longitudinally varying part of the inverse permittivity, evaluated at the jth carrier frequency.

C. Transverse modes

It is possible to solve the equation for $\mathbf{u}_{j\mathbf{m}}$ if Δ_{jr} is given, using the standard techniques for weakly guided waves at the jth carrier frequency. The modes $\mathbf{u}_{j\mathbf{m}}$ can also be normalized so that

$$\int\mathbf{u}_{j\mathbf{m}}\cdot\mathbf{u}_{j\mathbf{m}'}d^2\mathbf{r}=\delta_{\mathbf{m},\mathbf{m}'}. \tag{4.16}$$

These modes take different forms, depending on the specific type of waveguide.

(i) *One dimension:* In the one-dimensional case (for example, in a single mode fiber), higher order modes are usually neglected. We can write $\mathbf{u}_{j\mathbf{m}}$ simply as

$$\mathbf{u}_{j\mathbf{0}}=\mathbf{u}_{\mathbf{j}}(\mathbf{r}),$$

where $\mathbf{u}_{\mathbf{j}}$ is the zeroth order transverse mode, and the eigenvalue $\Delta\omega_{j\mathbf{m}}$ is $\Delta\omega_{j0}$.

Two dimensions: In a planar waveguide case (two dimensional), $\mathbf{u}_{j\mathbf{m}}$ can be written in the form

$$\mathbf{u}_{j\mathbf{m}}=\mathbf{u}_j(y)e^{ik_{jm}x}/\sqrt{L}$$

(assuming the waveguide is confined along the y direction, and L is the transverse normalization distance), where $\mathbf{u}_{\mathbf{j}}$ is the zeroth order transverse mode and k_{jm} is a scalar. Thus $\Delta\omega_{j\mathbf{m}}=\Delta\omega_{j0}+v_jk_{jm}^2/(2k_j)$, where $\Delta\omega_{j0}$ is the eigenvalue of the zeroth eigenmode.

Three dimensions: In a bulk crystal (three dimensional), $\mathbf{u_{jm}}$ can be written in the form

$$\mathbf{u_{jm}}=\mathbf{u}_j e^{i\mathbf{k_{jm}}\cdot\mathbf{r}}/L.$$

Here $\mathbf{u}_j$ is the polarization direction, $\Delta\omega_{j\mathbf{m}}=v_j|\mathbf{k_{jm}}|^2/(2k_j)$, and L^2 is the transverse normalization area.

D. Longitudinal modes

We next consider the longitudinal mode equation. We assume a waveguide which is longitudinally modulated in a similar manner as discussed in Sec. III, which defines ϵ_j. For frequencies in the neighborhood of the jth carrier frequency ω_j, the transversely averaged permittivity is defined as in the one-dimensional case:

$$\Delta_j(z)=\tilde{\epsilon}(z,\omega_j)/\overline{\epsilon}(\omega_j)-1=\sum_l \Delta_{jl}e^{2il\overline{k}z}+\text{c.c.} \tag{4.17}$$

The effective wave number $\overline{k}$ is the same as defined in Sec. III.

Expanding Λ_{jn} into a Fourier series, we look for modes that are described by a momentum factor Q_n such that

$$\Lambda_{jn}(z)=\lambda_{jn}\sum_l C_{jn}(k_{nl})\exp(ik_{nl}z), \tag{4.18}$$

where $k_{nl}=Q_n+l\overline{k}$ and l is an integer.

Substituting the above equation into Eq. (4.15) and collecting coefficients of terms with same wave numbers, we have the equation for the coefficients $C_{jn}(k)$:

$$\begin{aligned}(-k_{nl}^2\overline{\eta}_j+\mu_0\tilde{\omega}_{jn}^2)C_{jn}(k_{nl})&=k_{nl}\sum_{jl'}[(k_{nl}+2l'\overline{k})\overline{\eta}_j\Delta^*_{jl'}C_{jn}(k_{nl}+2l'\overline{k})\\&+(k_{nl}-2l'\overline{k})\overline{\eta}_j\Delta_{jl'}C_{jn}(k_{nl}-2l'\overline{k})].\end{aligned} \tag{4.19}$$

Solving the above equation yields the exact values of C_{jn} and the dispersion relationship between $\tilde{\omega}_{jn}$ and Q_n. Furthermore, for any two longitudinal modes, they must also satisfy the general orthonormality requirement [30,32,33]

$$\int\left(\Lambda^*_{jn}\Lambda_{jn'}-\frac{1}{2\mu_0\omega_{jn}}\frac{\partial\tilde{\eta}}{\partial\omega_{jn}}\partial_z\Lambda^*_{jn}\partial_z\Lambda_{jn'}\right)dz=\frac{L\hbar\delta_{nn'}}{2\mu_0\omega_{jn}}, \tag{4.20}$$

which determines the value of λ_{jn}, neglecting small terms corresponding to combined dispersive and transverse mode corrections. It is difficult to obtain the explicit form of Λ_{jn}, for it consists of an infinite series of terms whose coefficients are to be determined by infinite number of central equations [Eq. (4.19)].

We are interested in waves near the Bragg condition, for if the wave vector is too far away from the Bragg condition, the medium acts just like a homogeneous medium. We therefore assume $Q_n\ll\overline{k}$ and $\overline{\eta k_j^2}\approx\mu_0\tilde{\omega}_{jn}^2$. To treat these approximations, we will assume the solution can be expanded in a power series in the expansion parameter Δ, with $Q_n/\overline{k}<\Delta$. This allows us to group terms of the same order together, and neglect higher order terms in a consistent approach. To first order in this approximation, we retain only those equations that contain both coefficients $C_{jn}(\overline{k}+Q_n)$ and $C_{jn}(-\overline{k}+Q_n)$ since they dominate the other coefficients, which can then be neglected. This implies that we only retain terms in the expansion of Λ_{jn} with $l=\pm j$.

At this point, we notice, in the Fourier series for Λ_2, that the second-harmonic field interacts with Bragg gratings both with a resonant condition (Δ_{22}), and with a period of twice the resonant condition (Δ_{21}). In Eq. (4.19), we see that this subharmonic grating can only couple $C_{jn}(2\overline{k})$ to $C_{jn}(0)$ and $C_{jn}(4\overline{k})$. The corresponding coupling coefficient is zero for the coupling to $C_{jn}(0)$, due to the momentum factors, and therefore this nonresonant lattice does not result in Bragg reflections in the case of a volume Bragg grating. However, for surface Bragg gratings (not considered here) it is known that coupling to a subharmonic grating can cause large diffraction losses [34], due to scattering in orthogonal directions. This case of surface corrugations is therefore not treated here, as previously mentioned.

Equation Eq. (4.19) hence becomes (in the case of the jth carrier)

$$\begin{aligned}&[(j\overline{k}+Q_n)^2\overline{\eta}_j-\mu_0\tilde{\omega}_{jn}^2]C_{jn}(j\overline{k}+Q_n)\\&\quad+(Q_n{}^2-j^2\overline{k^2})\overline{\eta}_j\Delta_{jj}C_{jn}(-j\overline{k}+Q_n)=0,\\&(Q_n{}^2-j^2\overline{k^2})\overline{\eta}_j\Delta_{jj}C_{jn}(j\overline{k}+Q_n)\\&\quad+[(-j\overline{k}+Q_n)^2\overline{\eta}-\mu_0\tilde{\omega}_{jn}^2]C_{jn}(-j\overline{k}+Q_n)=0.\end{aligned} \tag{4.21}$$

Solving the above equation for $\tilde{\omega}_{jn}^2$, and including the explicit frequency dependence of the permittivity $\overline{\eta}(\omega)$, we have

$$\mu_0\tilde{\omega}_{jn}^2=(j^2\overline{k^2}+Q_n{}^2)\overline{\eta}_j+s\sqrt{(j^2\overline{k^2}-Q_n{}^2)^2|\overline{\eta}_j\Delta_{jj}|^2+4j^2\overline{k^2}Q_n{}^2\overline{\eta_j^2}}\approx j^2\overline{k^2}\overline{\eta}_j+s\sqrt{\overline{k^4}|\overline{\eta}_j\Delta_{jj}|^2+4j^2\overline{k^2}Q_n{}^2\overline{\eta_j^2}} \tag{4.22}$$

where the sign $s=-1$ corresponds to lower branch and $s=1$, upper branch.

This result agrees with a similar expression obtained by solving the linear Maxwell equation of the electric field and the permittivity [35]. The difference is of the order of the square of the expansion parameter (i.e., Δ^2), which can be neglected because both approaches only keep up to first order in Δ.

Taking the square root of both sides, and retaining terms to first order in Δ as before, we obtain

$$\tilde{\omega}_{jn}\approx v_p(\omega_j)(j\bar{k}+s\sqrt{|\kappa_j|^2+Q_n^2}), \tag{4.23}$$

where $v_p(\omega_j)=1/\sqrt{\mu_0\bar{\epsilon}(\omega_j)}$, and κ_j is defined as in the one-dimensional case, since $\kappa_j=j\bar{k}\Delta_{jj}/2$. We have used in this first order approximation, that the Bragg scattering term is nearly frequency independent within each band, i.e., $\kappa(\tilde{\omega}_{jn})\approx\kappa(\omega_j)\approx\kappa_j$.

If we substitute $\tilde{\omega}_{jn}=\omega_j+v_p(\omega_j)\Omega_{jn}/v_j$ into the above equation, we obtain the same dispersion relationship obtained in Eq. (3.5), so that

$$\Omega_{jn}=\Omega_j^{(s)}(Q_n)=v_j(s\sqrt{|\kappa_j|^2+Q_n^2}-\delta k_j), \tag{4.24}$$

where $\delta k_j=k(\omega_j)-j\bar{k}$ as before.

The longitudinal eigenvalue $\Omega_{j\mathbf{n}}$ is a function of Q_n, j and s, as are Λ_{jn} and C_{jn}. The total eigenvalue can be written as

$$\omega_{j\mathbf{n}}=\omega_{j\mathbf{m}}^{(s)}(Q_n)=\omega_j+\Delta\omega_{j\mathbf{m}}+\Omega_j^{(s)}(Q_n), \tag{4.25}$$

and we can write Λ_{jn} and C_{jn} as

$$\Lambda_{jn}(z)=\Lambda_j^{(s)}(Q_n,z)=\lambda_j^{(s)}(Q_n)u_{j\Lambda}^{(s)}(Q_n,z)e^{iQ_nz},$$

$$C_{jn}(\pm\bar{k}+Q_n)=C_{j\pm}^{(s)}(Q_n), \tag{4.26}$$

where the rapidly varying part of the Bragg grating mode function is given by

$$u_{j\Lambda[D]}^{(s)}(Q,z)=C_{j+}^{(s)}(Q)e^{ij\bar{k}z}+[-]C_{j-}^{(s)}(Q)e^{-ij\bar{k}z}. \tag{4.27}$$

Here $u_{j\Lambda}$ is the dual potential mode function, while u_{jD} is the displacement (or electric) field mode function in a slowly varying envelope approximation. From now on, we shall omit the longitudinal mode index on Q_n, since these modes become infinitely closely spaced in the limit of large quantization volume, where L is large.

The ratio between $C_{j+}^{(s)}(Q)$ and $C_{j-}^{(s)}(Q)$ is determined from Eq. (4.21). The coefficients $C_{j+}^{(s)}(Q)$ and $C_{j-}^{(s)}(Q)$ are normalized such that $(C_{j+}^{(s)}(Q))^2+(C_{j-}^{(s)}(Q))^2=1$. Using these conditions, we derive the explicit forms in the first order approximation,

$$C_{j\pm}^{(s)}(Q)=\pm f_{j\pm}^{(s)}(Q), \tag{4.28}$$

where $\vec{f}_j=(f_{j+},f_{j-})$ is the the same as in Eq. (3.7), in the section on the one-dimensional equation. There is an additional sign correction in the above equation, since the expansion given here is for the dual potential Λ, rather than in terms of the electric or displacement field. Once this is taken into account, the general symmetry properties of the longitudinal modes correspond exactly to those in the one-dimensional case.

The value of $\lambda_j^{(s)}(Q)$ can now be obtained from substituting $\Lambda_j^{(s)}(Q,z)$ into the normalization condition [30,32,33],

$$\frac{1}{L}\int\left[(\Lambda_j^{(s)})^*\Lambda_j^{(s)}-\frac{\tilde{\eta}'(z,\omega_{j\mathbf{m}}^{(s)}(Q))\partial_z(\Lambda_j^{(s)})^*\partial_z\Lambda_j^{(s)}}{2\mu_0\omega_{j\mathbf{m}}^{(s)}(Q)}\right]dz=\frac{\hbar}{2\mu_0\omega_{j\mathbf{m}}^{(s)}(Q)}, \tag{4.29}$$

where $\tilde{\eta}'(z,\omega)=\partial\tilde{\eta}/\partial z$.

Substituting Eq. (4.26) into the above equation, we find

$$(\lambda_j^{(s)}(Q))^2\left[(C_{j+}^{(s)}(Q))^2\left(1-\frac{1}{2\mu_0\omega_{j\mathbf{m}}^{(s)}(Q)}\bar{\eta}'(\omega_{j\mathbf{m}}^{(s)}(Q))(j\bar{k}+Q)^2\right)\right.$$

$$\left.+(C_{j-}^{(s)}(Q))^2\left(1-\frac{1}{2\mu_0\omega_{j\mathbf{m}}^{(s)}(Q)}\bar{\eta}'(\omega_{j\mathbf{m}}^{(s)}(Q))(-j\bar{k}+Q)^2\right)\right]=\frac{\hbar}{2\mu_0\omega_{j\mathbf{m}}^{(s)}(Q)}, \tag{4.30}$$

where we have used the approximation $\partial\tilde{\eta}(z,\omega)/\partial\omega \approx \partial\overline{\eta}(\omega)/\partial\omega$. We have assumed that Δ_j is dispersionless within its own frequency band. The dispersion $\tilde{\eta}'$ is normally small, and we suppose it is at most of order Δ in dimensionless units, i.e., we suppose that the product term $\tilde{\eta}'\overline{k}Q/(2\mu_0\omega_j)$ is of the order of Δ^2 and hence can be neglected. Using this approximation and solving Eq. (4.30) for $\lambda_j^{(s)}(Q)$ gives

$$\lambda_j^{(s)}(Q)\approx \sqrt{\frac{\hbar}{2\mu_0\omega_{j\mathbf{m}}^{(s)}(Q)-\overline{\eta}'(\omega_{j\mathbf{m}}^{(s)}(Q))j^2\overline{k}^2}}. \tag{4.31}$$

For later use, we need an approximate expression suitable for evaluating nonlinear interaction terms in the Hamiltonian. We therefore also evaluate this expansion coefficient at the gap center, giving the result

$$\lambda_j^{(s)}(0)\approx\lambda_j=\sqrt{\frac{\hbar v_j\overline{\epsilon}_j}{2k_j}}[1+O(\Delta)]. \tag{4.32}$$

In order to understand the physical properties of these solutions, we recall that these longitudinal mode functions are essentially identical in symmetry to those obtained in the one-dimensional case. Thus, if κ_j is real and positive, the lower energy displacement field solution for $Q=0$ (which is labeled as $s=-1$) has a $\cos(\overline{k}jz)$ spatial dependence, and is therefore completely symmetric about $z=0$. This can be understood physically by noticing that the linear Hamiltonian (ignoring all dispersion for simplicity), is given by

$$H_0=\int\sum_j\left(\frac{1}{\mu_0}|\vec{\mathcal{B}}_j|^2+\eta(\mathbf{x})|\vec{\mathcal{D}}_j|^2\right)d^3\mathbf{x}. \tag{4.33}$$

In the case that κ_j is real and positive, the inverse dielectric permittivity has a negative $\cos(2\overline{k}jz)$ modulation term, which reduces the energy of the symmetric $\cos(\overline{k}jz)$ field mode, with $s=-1$, while increasing the energy of the antisymmetric mode with $s=1$.

These energy changes agree precisely with the frequency changes of the mode frequencies worked out from the solutions to the one-dimensional Maxwell equations. While this is as expected, it provides an additional confirmation of the correctness of the Hillery-Mlodinow form of the dielectric-radiation Hamiltonian that is used here. This difference in energy is, of course, the physical origin of the band gap in the dispersion relations.

V. EFFECTIVE-MASS APPROXIMATION

In the above analysis, we have assumed that both $Q/\overline{k}$ and Δ_{jj} are first order in a dimensionless expansion parameter Δ. We are now interested in photon properties near the center of the band-gap region in momentum space, where Q is small, so we further assume here that $Q/\kappa\ll 1$. This is a different expansion parameter to Δ, and in practical terms can be much larger than Δ in many cases. We emphasize that the expansion is not essential to the problem—we can still write down the Hamiltonian without it—but it greatly simplifies the final equations that are obtained. We first expand $\omega^{(s)}(Q)$ around the carrier frequency ω_j. This gives the dispersion relationship [Eq. (3.5)], which was obtained from the coupled mode theory. We then expand the resulting expression in a Taylor series up to second order in $Q/|\kappa_j|$:

$$\Omega_j^{(s)}(Q)=\Omega_j^{(s)}(0)+\frac{s\hbar Q^2}{2m_j}, \tag{5.1}$$

where the effective mass of the jth carrier is

$$m_j=\hbar|\kappa_j|/v_j, \tag{5.2}$$

and v_j is the group velocity. The frequency at the band-gap edge is

$$\Omega_j^{(s)}(0)=(s|\kappa_j|-\delta k_j)v_j. \tag{5.3}$$

This is, in fact, the well-known effective-mass approximation (EMA) in solid state physics—although more precisely sm_j is called the effective mass, with opposite signs below and above the band gap. It should be noticed here that the main effect of material group-velocity terms is to slightly change the curvature of the effective-mass parabola. This term is therefore much less significant for modes near the band center, whose effective group velocities in essence are due to the Bragg grating itself.

It can be shown that the remainder term of the above expansion is

$$R^{(3)}(Q)=\frac{-\hbar s|\kappa_j|^2v_jQ^4}{2(|\kappa_j|^2+Q^2)^{5/2}}. \tag{5.4}$$

The condition that the EMA is valid is then

$$|R^{(3)}(Q)|\ll\left|\frac{\hbar^2Q^2}{2m_j}\right|. \tag{5.5}$$

The above condition can be easily satisfied if $Q<|\kappa_j|$. The value of the remainder term is significant compared with the value of the second term only if Q and $|\kappa_j|$ are of similar magnitudes.

The total eigenvalue, $\omega_{j\mathbf{n}}$, of the mode equation is the sum of the longitudinal eigenvalue $\omega_j+\Omega_{jn}$, and the transverse eigenvalue, $\Delta\omega_{j\mathbf{m}}$. From this relationship we have (near the jth carrier)

$$\omega_{j\mathbf{n}}=\omega_{j\mathbf{m}}^{(s)}(Q_n)=\omega_{j\mathbf{m}}^{(s)}+\frac{s\hbar Q_n^2}{2m_j}, \tag{5.6}$$

where the eigenvalue at the band-gap edge is

$$\omega_{j\mathbf{m}}^{(s)}=\omega_j+\Omega_j^{(s)}(0)+\Delta\omega_{j\mathbf{m}}. \tag{5.7}$$

It is convenient to work in the coordinate representation if we want to compare theoretical results to those of experiments. The Hamiltonian can therefore be expressed in terms of these field operators. We introduce an effective dimensionality $D=1,2$, and 3. As usual, we first consider the linear part of the Hamiltonian describing waveguides with confinement in two transverse dimensions ($D=1$) and in one transverse dimension ($D=2$), as well as bulk crystals ($D=3$)

which have no transverse confinement (except boundary conditions). To simplify the analysis, we assume that where there are discrete transverse modes—as in a fiber—only the lowest order mode $[\mathbf{m}=(0,0)]$ needs to be considered. In this case, we define $\omega_j^{(s)}=\omega_{j\mathbf{0}}^{(s)}$. The restriction to single discrete transverse modes is not always possible, and depends on the mode level spacing.

We introduce an envelope for the excitation in the dielectric—which physically is really the polariton density field—in D dimension(s), defined as

$$\Psi_j^{(s)}(\mathbf{x})=L^{-D/2}\sum_{\mathbf{k}} a_{j\mathbf{k}}^{(s)}e^{i\mathbf{k}\cdot\mathbf{x}}, \tag{5.8}$$

where $\mathbf{k}=(0,0,Q)$ in one dimension, $\mathbf{k}=(k_{jm},0,Q)$ in two dimensions, and $\mathbf{k}=(\mathbf{k}_{jm},Q)$ in three dimensions.

The inverse Fourier transform of the above expression is

$$a_{j\mathbf{k}}^{(s)}=L^{-D/2}\int d^D\mathbf{x}\Psi_j^{(s)}(\mathbf{x})e^{-i\mathbf{k}\cdot\mathbf{x}}, \tag{5.9}$$

where $\mathbf{x}=(\mathbf{r},z)$ as before.

Substituting the above expression together with Eq. (5.7) into the linear part of the Hamiltonian, we have

$$H_0\approx\sum_{j,s}\hbar\int\left(\frac{s\hbar}{2m_j}|\partial_z\Psi_j^{(s)}|^2+\frac{\hbar}{2m_{j\perp}}|\nabla_{D\perp}\Psi_j^{(s)}|^2+\omega_j^{(s)}|\Psi_j^{(s)}|^2\right)d^D\mathbf{x}, \tag{5.10}$$

where $\nabla_{D\perp}$ is the transverse part of the operator in D dimensions, so that $\nabla_{3\perp}=(\partial/\partial x,\partial/\partial y)$, and $m_{j\perp}=\hbar k_j/v_j$ is the effective transverse mass. We notice that typically, $m_{2\perp}\simeq 2m_{1\perp}$ to a good approximation, although this is not a requirement in the theory. The longitudinal and transverse effective masses often can have quite different values, especially if the Bragg dispersion is large (i.e., $|\kappa_j|$ is small). Thus, given the parameters quoted in Sec. III, the effective masses have the following orders of magnitude: $m_j\sim 10^{-38}$ kg and $m_{j\perp}\sim 10^{-35}$ kg.

Nonlinear part of the Hamiltonian

For solitons, the nonlinear part of the Hamiltonian is about the same order as the ''dispersive terms'' (terms involving $\partial^2/\partial z^2$), since the cancellation of nonlinearity and dispersion is the requirement for soliton formation. This indicates that we only need to keep the leading terms, when we use the EMA to expand $\mathcal{D}$ in a series of $Q/|\kappa_j|$ for the nonlinear part of the Hamiltonian. Assuming that $\mathbf{u_{jm}}$ is slowly varying, we therefore have, approximately,

$$\vec{\mathcal{D}}=\frac{1}{\sqrt{L}}\sum_{j\mathbf{n}}(\nabla\Lambda_{j\mathbf{n}}\times\mathbf{u_{jm}}+\Lambda_{j\mathbf{n}}\nabla\times\mathbf{u_{jm}})a_{j\mathbf{n}},$$

$$\approx\frac{1}{\sqrt{L}}\sum_{j\mathbf{n}}\nabla\Lambda_{j\mathbf{n}}\times\mathbf{u_{jm}}. \tag{5.11}$$

Substituting Eq. (4.26) into the above equation, we have

$$\vec{\mathcal{D}}_j\approx iL^{-D/2}\hat{\mathbf{z}}\times\mathbf{u}_j(\mathbf{r})\sum_{s,\mathbf{k}}\lambda_j^{(s)}(Q)[(j\bar{k}+Q)C_{j+}^{(s)}(Q)e^{ij\bar{k}z}+(Q-j\bar{k})C_{j-}^{(s)}(Q)e^{-ij\bar{k}z}]a_{j\mathbf{k}}^{(s)}e^{i\mathbf{k}\cdot\mathbf{x}}. \tag{5.12}$$

For simplicity, we take the above equation to the limit of $Q=0$, thus eliminating cross coupling terms involving Q (which are smaller than the zeroth order terms):

$$\vec{\mathcal{D}}_j\approx i\mathbf{e}_j(\mathbf{r})\sum_s\lambda_j j\bar{k}u_{jD}^{(s)}(0,z)\Psi_j^{(s)}(\mathbf{x})+O(Q/\kappa_j)$$

$$\approx i\frac{\sqrt{\hbar k_j\bar{\epsilon}_j v_j}}{2}\sum_s[\mathrm{sgn}(\kappa_j)e^{ij\bar{k}z}-se^{-ij\bar{k}z}]\Psi_j^{(s)}(\mathbf{x})\mathbf{e}_j(\mathbf{r}), \tag{5.13}$$

where $\mathbf{e}_j(\mathbf{r})=\hat{\mathbf{z}}\times\mathbf{u}_j(\mathbf{r})$ is the transverse mode polarization vector [in a three-dimensional case, $\mathbf{e}_j(\mathbf{r})$ becomes independent of $\mathbf{r}$], and $\mathrm{sgn}(x)=x/|x|$ is a complex function that becomes the sign function if x is real.

We next proceed to the nonlinear part of the Hamiltonian. Substituting the above expression into the nonlinear part of the Hamiltonian results in

$$H_{\mathrm{int}}\approx-\frac{\hbar}{2}\sum_{\vec{s}}\int\chi(\vec{s})(\Psi_2^{(s_2)})^*\Psi_1^{(s_1)}\Psi_1^{(s_1')}d^D\mathbf{x}+\mathrm{H.c.}, \tag{5.14}$$

where the nonlinear coupling is:

$$\chi(\vec{s})=\frac{i\epsilon_0 k_1 v_1}{4\bar{\epsilon}_1}\sqrt{\frac{\hbar k_2 v_2}{\bar{\epsilon}_2}}[\mathrm{sgn}(\kappa_2)^*\mathrm{sgn}(\kappa_1)\mathrm{sgn}(\kappa_1')-s_1s_1's_2]\int\mathbf{e}_2^*(\mathbf{r})\cdot\chi^{(2)}:\mathbf{e}_1(\mathbf{r})\mathbf{e}_1(\mathbf{r})d^{(3-D)}\mathbf{r}. \tag{5.15}$$

The nonlinear part of the Hamiltonian [Eq. (5.14)], vanishes if the total coupling between gaps is antisymmetric. We only consider cases with nonvanishing coupling, and $s_1=s_1'$, although, in a three-wave mixing process, it is possible that $s_1\neq s_1'$. This condition limits the number of possible couplings. Therefore, these possible couplings between gaps are (1) coupling between lower branches, (2) coupling between upper branches, and (3) coupling between upper and lower branches, as illustrated in Fig. 2. We can always assume κ_1 to be real and positive, by shifting the location of the coordinate origin, since only the relative phase between the two gratings is important. The nonlinear coupling is now simplified to

$$\chi(\vec{s})=\frac{i\chi_E v_1}{4}\sqrt{\frac{\hbar k_2 v_2}{\epsilon_2 A_c}}[\mathrm{sgn}(\kappa_2)^*-s_2], \qquad (5.16)$$

where an effective mode ''area'' A_c (or ''width'' if $D=2$) is defined for $D<3$, as

$$A_c=\left|\frac{\mathbf{e}_2^*(0)\cdot\chi^{(2)}:\mathbf{e}_1(0)\mathbf{e}_1(0)}{\int\mathbf{e}_2^*(\mathbf{r})\cdot\chi^{(2)}:\mathbf{e}_1(\mathbf{r})\mathbf{e}_1(\mathbf{r})d^{(3-D)}\mathbf{r}}\right|^2. \qquad (5.17)$$

We now suppose that κ_2 is also real, but can have either sign. This would be the case if the overall grating structure was symmetric relative to the origin. We can investigate the possible cases of modes having a nonzero coupling at $Q=0$, by simply considering whether $[\mathrm{sgn}(\kappa_2)-s_2]$ is zero or not. Thus, it is clear that only the second harmonic mode is restricted in any way, and in this case it is necessary that s_2 has the opposite sign to κ_2. However, as discussed earlier, this is precisely the condition for having a symmetric modal solution. In summary, while the parity of the fundamental harmonic can have either sign, the parity of the second harmonic must be symmetric. We can understand the physics of this in a very straightforward way. The nonlinear coupling involves the square of the fundamental field, multiplied by the second harmonic. The square of the fundamental field mode is always symmetric whether the mode itself is symmetric or antisymmetric. This can only give rise to a finite nonlinear coupling if the second-harmonic mode is also symmetric about $z=0$.

The Hamiltonian approach therefore affords a physically intuitive understanding of the coupling processes and a more accurate description of physics involved with transverse modes (which was omitted in the simplified one-dimensional coupled mode analysis). Not only does the use of the gap modes eliminate linear cross couplings, but it also introduces a powerful symmetry principle in the limit of $Q=0$; the second harmonic that is coupled must have the same type of symmetry as the product of the two subharmonic modes. Because of this, the use of gap modes permits great simplifications even in this nonlinear problem. Either quantum soliton [36] or classical soliton behavior can result; the classical solutions would, of course, be approximately valid only at large photon number. However, this technique does permit us to obtain solutions of some experimental interest.

VI. DIMENSIONLESS EQUATIONS

In order to obtain solutions to Eq. (2.12), we need to obtain a coupled mode equation from the Hamiltonian, which we call the Hamiltonian classical equation. This proves to have a much simpler form than before, and can be reduced to just two coupled dimensionless nonlinear equations. The advantage is that the final equations have been extensively analyzed in previous work. Since both approaches describe similar physics, the solutions to the Hamiltonian classical equation should also be approximately the solutions of Eq. (2.12), apart from the simplifications introduced by the EMA. Equation (2.12) also did not consider effects introduced by transverse modes. In order to obtain solutions identical with Eq. (2.12), we could omit transverse mode terms involving $\Delta\omega_j$ in the Hamiltonian.

When these terms are necessary, they simply correspond to a renormalization of the linear phase-matching and dispersion properties of the medium. This well-known phenomenon is usually termed modal dispersion, and is typically rather small, except near the transverse mode cutoff frequencies. The other effects introduced by the full three-dimensional analysis (even for a one-dimensional waveguide or fiber) is that the coupling is now given in general by a transverse integral over the mode functions, and in the higher-dimensional waveguides there is an additional coupling between the different transverse modes. This corresponds to Eq. (2.12) only when additional Laplacian terms are included, as we will see.

A. Hamiltonian classical equation

Combining the above results, the approximate EMA Hamiltonian is now

$$H/\hbar\approx\sum_{j,s}\int\left(\frac{s\hbar}{2m_j}|\partial_z\Psi_j^{(s)}|^2+\frac{\hbar}{2m_{j\perp}}|\nabla_{D\perp}\Psi_j^{(s)}|^2+\omega_j^{(s)}|\Psi_j^{(s)}|^2\right)d^D\mathbf{x}-\left[\frac{1}{2}\sum_s\int\chi(\vec{s})(\Psi_2^{(s_2)})^*\Psi_1^{(s_1)}\Psi_1^{(s_1')}d^D\mathbf{x}+\mathrm{H.c.}\right]. \qquad (6.1)$$

The classical (coherent or mean field) evolution can be calculated from the Poisson bracket

$$\frac{\partial\Psi_j}{\partial t}=\{\Psi_j,H\}, \qquad (6.2)$$

where the canonical momentum field conjugate to Ψ is $i\hbar\Psi^*$. Substituting the EMA Hamiltonian into the above equation, we derive classical equations for coupled waves with general symmetry properties:

$$\frac{\partial\Psi_1^{(s_1)}}{\partial t}=i\left[\frac{s_1\hbar}{2m_1}\frac{\partial^2}{\partial z^2}+\frac{\hbar}{2m_{1\perp}}\nabla_{D\perp}^2-\omega_1^{(s_1)}\right]\Psi_1^{(s_1)}+\sum_{s_1'}i\chi^*(\vec{s})\Psi_2^{(s_2)}(\Psi_1^{(s_1')})^*,$$

$$\frac{\partial\Psi_2^{(s_2)}}{\partial t}=i\left[\frac{s_2\hbar}{2m_2}\frac{\partial^2}{\partial z^2}+\frac{\hbar}{2m_{2\perp}}\nabla_{D\perp}^2-\omega_2^{(s_2)}\right]\Psi_2^{(s_2)}+\sum_{s_1s_1'}\frac{i\chi(\vec{s})}{2}\Psi_1^{(s_1)}\Psi_1^{(s_1')}. \qquad (6.3)$$

To compare these equations with previously known results, we suppose that only a definite pair of gap modes are excited in $D=1$ dimensions, having symmetries s_1 and s_2, respectively. In this case, it is convenient to define slowly varying fields: $\psi_1=\Psi_1^{(s_1)}e^{i(\omega t-kz)}$ and $\psi_2=\Psi_2^{(s_2)}e^{2i(\omega t-kz)}$. We also consider a new frame of reference moving (slowly) at velocity v in the laboratory frame—with a new z coordinate $z_v=z-vt$—while still remaining within the effective-mass approximation. With this frame transformation, we must replace ∂_t by $\partial_t-v\partial_{z_v}$. To simplify the resulting equations, we set

$$\omega=\omega_1^{(s_1)}+\tfrac{1}{2}s_1m_1v^2/\hbar,\qquad k=m_1s_1v/\hbar. \tag{6.4}$$

A pair of new equations in the moving reference frame is obtained:

$$\frac{\partial\psi_1}{\partial t}=i\frac{s_1\hbar}{2m_1}\frac{\partial^2\psi_1}{\partial z_v^2}+i\chi^*(\vec{s})\psi_2\psi_1^*,$$

$$\left[\frac{\partial}{\partial t}-\Delta v\frac{\partial}{\partial z_v}\right]\psi_2=i\frac{s_2\hbar}{2m_2}\frac{\partial^2\psi_2}{\partial z_v^2}+i\beta_v(s_1,s_2)\psi_2+i\frac{\chi(\vec{s})}{2}\psi_1^2. \tag{6.5}$$

This is of the identical form to the usual description of a nonlinear dispersive parametric waveguide, with effective dispersions

$$\omega''_{j\mathrm{EFF}}=s_j\hbar/m_j, \tag{6.6}$$

an effective phase mismatch of

$$\begin{aligned}\beta_v(s_1,s_2)&=(2\omega_1^{(s_1)}-\omega_2^{(s_2)})+\frac{m_1v^2}{\hbar}\left(s_1-\frac{2m_1s_2}{m_2}\right)\\&=2(s_1|\kappa_1|-\delta k_1)v_1-(s_2|\kappa_2|-\delta k_2)v_2\\&\quad+\frac{m_1v^2}{\hbar}\left(s_1-\frac{2m_1s_2}{m_2}\right),\end{aligned} \tag{6.7}$$

and a group-velocity mismatch of

$$\Delta v=v(1-2m_1s_1s_2/m_2). \tag{6.8}$$

These equations have been extensively analyzed previously [1–19], in the context of the propagation of simultons in ordinary, nonmodulated parametric material. In this earlier situation, the roles of t and z were reversed, with the analysis taking place in a moving reference frame at close to the material group velocity. Nevertheless, the mathematical properties of these earlier nonlinear equations can now be used to analyze the more complex gap parametric soliton case. A similar transformation is possible in the NLS problem, where an approximate NLS equation can be used to treat gap solitons under certain conditions. From these previously known results [16], Eqs. (6.5) support dark (i.e., topological) solitary waves if $s_1=-s_2$ (coupling between the upper branch and the lower branch). Also, bright type solitary waves can occur, if the dispersions have identical sign, i.e., $s_1=s_2$ (coupling between upper branches *or* lower branches). From Eqs. (6.8) it appears that this condition is also required in order to have moving solutions that are form invariant with respect to the stationary ones. Clearly, only if $s_1=s_2$ is it possible for the group-velocity terms to vanish in the moving-frame equations. It is also possible that there could be moving topological solitons with properties that depend on velocity. However, this will not be investigated here.

Similarly, higher-dimensional equations can be obtained. In this case, the previous definitions are extended in the obvious way, so that

$$\psi_1=\Psi_1^{(s_1)}e^{i(\omega t-\mathbf{k}\cdot\mathbf{x})},\qquad \psi_2=\Psi_2^{(s_2)}e^{2i(\omega t-\mathbf{k}\cdot\mathbf{x})}. \tag{6.9}$$

The new frame of reference moves at velocity $\mathbf{v}$ in the laboratory frame, with a new x-coordinate: $\mathbf{x_v}=(\mathbf{r_v},z_\mathbf{v})=\mathbf{x}-\mathbf{v}t$. The frequencies and wave numbers appropriate to this transformation are [with $\mathbf{v}=(\mathbf{v}_\perp,v_z)$]

$$\omega=\omega_1^{(s_1)}+\tfrac{1}{2}s_1m_1v_z^2/\hbar+\tfrac{1}{2}m_{1\perp}|\mathbf{v}_\perp|^2/\hbar,\qquad k_z=m_1s_1v/\hbar,\qquad \mathbf{k}_\perp=m_{1\perp}\mathbf{v}_\perp s_1/\hbar. \tag{6.10}$$

We see immediately that there is a very simple physical interpretation of the altered frequency equation for ω. The photon polaritons behave as classical particles, with an effective longitudinal mass of s_jm_j and a transverse mass of $m_{j\perp}$. It is therefore necessary to supply a kinetic energy of $mv^2/2$ in order to excite them into motion. This is modified from the usual classical result, since the transverse and longitudi-

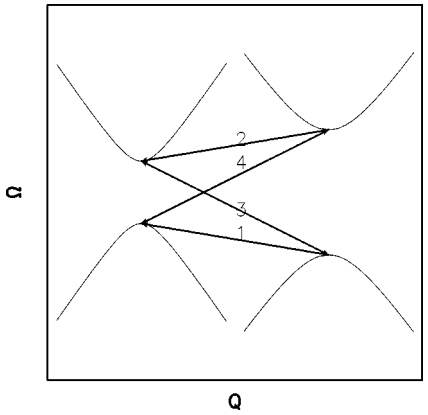

FIG. 2. Possible nonlinear couplings between gaps. Couplings 1 and 2 generate bright simultons, while couplings 3 and 4 generate dark simultons.

nal masses can be different. In addition, the longitudinal mass below the band gap is $-m_j$, so the ''kinetic energy'' is negative in this case. We note, for future reference, that below the band gap the longitudinal and transverse masses have opposite signs, which implies that there is no coordinate rescaling that can give rotationally symmetric equations.

This transformation gives new, moving frame equations in the form

$$\frac{\partial \psi_1}{\partial t} = i\frac{s_1\hbar}{2m_1}\frac{\partial^2\psi_1}{\partial z_v^2} + i\frac{\hbar}{2m_{1\perp}}\nabla_{D\perp}^2\psi_1 + i\chi^*(\vec{s})\psi_2\psi_1^*,$$

$$\left[\frac{\partial}{\partial t} - \Delta\mathbf{v}\cdot\nabla_{z_v}\right]\psi_2 = i\frac{s_2\hbar}{2m_2}\frac{\partial^2\psi_2}{\partial z_v^2} + i\frac{\hbar}{2m_{2\perp}}\nabla_{D\perp}^2\psi_2 + i\beta_{\mathbf{v}}(s_1,s_2)\psi_2 + i\frac{\chi(\vec{s})}{2}\psi_1^2, \tag{6.11}$$

where $\nabla_{2\perp}^2 = \partial^2/\partial_{x_v}^2$ for two dimensions, and $\nabla_{3\perp}^2 = \partial^2/\partial_{x_v}^2 + \partial^2/\partial_{y_v}^2$ for three dimensions. The effective phase mismatch is now

$$\begin{aligned}\beta_{\mathbf{v}}(s_1,s_2) &= (2\omega_1^{(s_1)} - \omega_2^{(s_2)}) + \frac{m_1 v_z^2}{\hbar}\left(s_1 - \frac{2m_1 s_2}{m_2}\right) + \frac{m_{1\perp}|\mathbf{v}_\perp|^2}{\hbar}\left(1 - \frac{2m_{1\perp}}{m_{2\perp}}\right)\\ &= 2(s_1|\kappa_1| - \delta k_1)v_1 - (s_2|\kappa_2| - \delta k_2)v_2 + \frac{m_1 v^2}{\hbar}\left(s_1 - \frac{2m_1 s_2}{m_2}\right) + \frac{m_{1\perp}|\mathbf{v}_\perp|^2}{\hbar}\left(1 - \frac{2m_{1\perp}}{m_{2\perp}}\right),\end{aligned} \tag{6.12}$$

and an effective group-velocity mismatch of $\Delta\mathbf{v} = (\Delta\mathbf{v}_\perp, \Delta v_z)$, where

$$\Delta v_z = v_z(1 - 2m_1 s_1 s_2/m_2),$$

$$\Delta\mathbf{v}_\perp = \mathbf{v}_\perp(1 - 2m_{1\perp}/m_{2\perp}). \tag{6.13}$$

B. Transforming to dimensionless equations

In the following sections, we consider cases with κ_j being real for simplicity. We will usually deal with a ''standard'' case, in which $s_1 = 1$ for simplicity. Other cases can be treated by considering more general transformations, but may not always lead to solitons—except in one dimension, where the positive and negative dispersion cases are related by a conjugation transformation.

The solution form of Eqs. (6.5) and (6.11) is known [16,21]. Soliton-type solutions can be most readily obtained by transforming to a standard, dimensionless form. We choose a transformation similar to that given in an earlier analysis of multidimensional solutions in uniform parametric media [21]:

$$V_1(\boldsymbol{\rho},\zeta,\tau) = |\chi(\vec{s})|t_c\sqrt{\sigma}e^{-iqt}\psi_1(\mathbf{x}_\mathbf{v},t),$$

$$V_2(\boldsymbol{\rho},\zeta,\tau) = \chi(\vec{s})s_1 t_c e^{-2iqt}\psi_2(\mathbf{x}_\mathbf{v},t), \tag{6.14}$$

where V_j are dimensionless envelope functions describing soliton shapes, and σ is defined by $\sigma = m_2/m_1$ in one dimension, and $\sigma = m_{2\perp}/m_{1\perp} \simeq 2$ in higher dimensions. The coordinate transform is defined in terms of a characteristic soliton length z_c, and has the obvious forms

$$\boldsymbol{\rho} = \mathbf{r}_\mathbf{v}/r_c,$$

$$\zeta = z_v/z_c, \tag{6.15}$$

$$\tau = t/t_c.$$

Once z_c is specified, the other characteristic length and time scales can be calculated from

$$t_c = 1/|q| = 2m_1 z_c^2/\hbar = 2|\kappa_1|z_c^2/v_1, \tag{6.16}$$

$$r_c = z_c\sqrt{m_1/m_{1\perp}} = z_c\sqrt{|\kappa_1|/k_1}.$$

The parameter $q = s_1/t_c$ has an important and very clear physical significance. It represents the additional detuning of the carrier frequency required to launch a soliton. Thus the previous definition of the fundamental carrier frequency ω gives a frequency which corresponds to either the upper ($s_1 = 1$) or lower ($s_1 = -1$) boundary of the band gap, together with a correction for a finite velocity excitation. The offset freqency q is a nonlinear effect, and typically brings the carrier frequency into the band-gap region, where linear mode propagation is not possible. This controls the appropriate soliton intensity (since the effect is nonlinear) and the appropriate envelope size (since dispersion and diffraction have to cancel some nonlinear phase shifts), as well as the interaction time scale. In practical terms, the characteristic input pulse duration is set by z_c, since this determines the pulse length.

For the two modes in this Hamiltonian EMA approximation, the most studied cases are for matching group velocities. This can be achieved either at zero pulse velocity in the laboratory frame (in all cases), or else at finite pulse velocity—but with $\Delta\mathbf{v} = 0$, so that $m_2 = 2m_1$ in the required motional direction. This simply requires that material group velocities be matched in the transverse motion case. However, for longitudinal motion, the requirements translate into restrictions on the band-gap-induced dispersion—and hence on the modulated refractive index. That is, we must have $|\Delta_{22}|/v_2 = |\Delta_{11}|/v_1$ for moving solutions in the z direction, together with the requirement that $s_1 = s_2$, as already mentioned. For simplicity, only these cases will be treated at nonzero velocity, thus allowing us to remove the group-velocity mismatch term.

The resulting moving-frame dimensionless equations are

$$(i\partial_\tau+\partial_\zeta^2+s_1\nabla_{\rho\perp}^2-1)V_1+V_2V_1^*=0,$$
$$(i\sigma\partial_\tau+\delta\partial_\zeta^2+s_1\nabla_{\rho\perp}^2-\gamma)V_2+\frac{1}{2}V_1^2=0. \tag{6.17}$$

Here we have introduced two new dimensionless parameters γ and δ, which characterize a family of solitons. γ indicates a type of renormalized phase mismatch, which depends both on the characteristic length and the material properties. In analogy with previous studies, we use δ to indicate a lack of symmetry in the band-gap curvature between the two frequencies. The exact definitions of the dimensionless parameters are

$$\delta=\sigma(m_1s_1s_2/m_2),$$
$$\gamma=\sigma(2-\beta/q). \tag{6.18}$$

In one space dimension, $D=1$, we have $\delta=\pm1$.

For a laser pulse of the order of 10 ps, we estimate $z_c=v_1\times10^{-11}$ s is of the order of 10^{-3} m. Since $Qz_c\approx1$ for a transform limited pulse, Q is then of the order of 10^3 m^{-1}. This is much smaller than κ_j when κ_j is of the order of 10^4 m^{-1}, as estimated previously. The validity of the EMA is therefore well justified for these parameters. For theoretical studies, the condition, $Q\ll\kappa_j$, can also be understood as $2q/v_1\ll\kappa_1$ or $\kappa_1z_c\gg1$. Provided these restrictions are met, the previously known analyses of solitary wave formation and stability for the coupled equations given above can be used.

In order to compare the above solutions with the classical equations obtained from the coupled mode analysis, we need to write the electric field in terms of Ψ_j. In a first approximation, we only keep the leading terms in the expansion of E in terms of D; this is justified when the refractive index modulation is relatively small,

$$\mathcal{E}_j\approx\overline{\eta_j}\mathcal{D}_j. \tag{6.19}$$

On the basis of the condition $Q\ll\kappa_j$, we can expand the mode function $C_{j\pm}^{(s)}(Q)$ into a Taylor series up to first order about $Q=0$. Hence, the electric field can be expressed as

$$\vec{\mathcal{E}}_j=i\sum_s\sqrt{\frac{\hbar k_jv_j}{2\epsilon_j}}\left(\Psi_j^{(s)}u_{jD}^{(s)}(0,z)-i\frac{\partial\Psi_j^{(s)}}{\partial z}\frac{\partial u_{jD}^{(s)}(0,z)}{\partial Q}\right)\mathbf{e}_j(\mathbf{r})+O(Q^2/\kappa_j^2), \tag{6.20}$$

where, as previously, $u_{jD}^{(s)}(Q,z)=C_{j+}^{(s)}(Q)e^{ij\overline{kz}}-C_{j-}^{(s)}(Q)e^{-ij\overline{kz}}$.

The pulse energy for a narrow-band excitation can be obtained by noticing that the D-dimensional volume integral of $|\Psi_j^2|$ is simply the total number of photons at angular frequency ω_j. This means we have to compute the pulse energy integral

$$W=\int(\hbar\omega_1|\Psi_1|^2+\hbar\omega_2|\Psi_2|^2)d^D\mathbf{x}$$
$$=z_cr_c^{(D-1)}A_cW(z_c)\int\int(V_1^2/\sigma+2V_2^2)d\zeta d^{(D-1)}\boldsymbol{\rho}, \tag{6.21}$$

where $W(z_c)$ gives the energy density requirement for a given soliton length scale z_c, through the relation

$$W(z_c)=\hbar\omega_1/(A_c|\chi(\vec{s})t_c|^2)=\frac{\varepsilon_2\overline{kc}^4}{2v_2\omega_1(\tilde{\chi}^{(2)}\kappa_1z_c^2\omega_1)^2}. \tag{6.22}$$

VII. GAP SIMULTONS

Having reduced the original system of four coupled partial differential equations to just two equations in the EMA limit, we can now analyze the situation for solitonic behavior. This is a straightforward exercise, since the final dimensionless equations correspond to a well-known traveling-wave nonlinear wave equation, and are known to have a variety of soliton-type solutions. Exactly which solution exists, and what stability properties are expected, will depend on the coupling parameters and dimensionality of the equations. Unlike the nonlinear Schrödinger equation, the solutions in this case are not all self-similar—there are many different possibilities that can occur. In general, solitons prove simplest to form in one dimension. As we will show, the question of whether or not a soliton can form in higher dimensions depends on the structure of the Bragg grating.

A. One-dimensional gap simultons

We start by comparing the EMA equations with the original one-dimensional band-gap equations. First, substitute Eq. (6.14) into the equation for the electric field, regarding the mode vectors $\mathbf{e}_j(\mathbf{r})=\hat{\mathbf{z}}\times\mathbf{u}_j(\mathbf{r})$ as the polarization vectors divided by $\sqrt{A_c}$ (i.e., $\mathbf{e}_j/\sqrt{A_c}$), where A_c is the mode confinement are. This is necessary because the coupled equation obtained from the original one-dimensional Maxwell equation did not consider transverse behavior. Comparing the resulting equation with Eq. (2.5) at $z=0$, we have (for nonmoving simultons):

$$\vec{\mathcal{A}}_1^{(s_1)}\approx\pm a_1\left(V_1\begin{bmatrix}\mathrm{sgn}(\kappa_1)\\-s_1\end{bmatrix}-\frac{i}{2|\kappa_1|}\frac{dV_1}{dz}\begin{bmatrix}\mathrm{sgn}(\kappa_1)s_1\\1\end{bmatrix}\right),$$
$$\vec{\mathcal{A}}_2^{(s_2,s_1)}\approx a_2\left(s_1V_2\begin{bmatrix}1\\1\end{bmatrix}-\frac{is_1s_2}{2|\kappa_2|}\frac{dV_2}{dz}\begin{bmatrix}1\\-1\end{bmatrix}\right). \tag{7.1}$$

Here $a_1=\sqrt{|\kappa_1/2\kappa_2|}|q|e^{i(q-\omega_1^{(s_1)})t}/(\chi_Ev_1)$ and $a_2=|q|e^{2i(q-\omega_1^{(s_1)})t}/(\chi_Ev_1)$.

It has been proved that there is a family of one parameter solitary wave solutions of Eq. (6.5) [16]. Provided that the effective-mass approximation is valid, each of these known simultaneous solitary waves (simultons) generates a corresponding band-gap soliton. Depending on the signs of s_1 and s_2, these solutions can be classified as topological and nontopological simultons. The general classification into various types of soliton is already known, and the details are pre-

sented elsewhere [16]. We note here that all the previously described types of soliton can be obtained under different conditions of interband coupling. In addition, new types may be obtained as it is possible to have intrinsic three-wave (nondegenerate) solitons by coupling both above and below the band gap. However, these generalizations will not be considered here.

A family of nontopological gap simultons to Eq. (6.5) exists for general values of γ when the signs of s_j are same. This corresponds to $s_1=s_2=-\mathrm{sgn}(\kappa_2)$, in order to have a nonzero coupling. We are mostly interested in cases where $s_1=1$, since this leads to a positive longitudinal mass, and hence to stable higher-dimensional solitons. Clearly, this would require that $\kappa_2<0$. However, in one dimension, conditions are less strict, and the restriction of $\kappa_2<0$ is not required for soliton formation.

In the special case of $\gamma=1$, the solutions are given in analytic form as

$$V_1(z)=\frac{3}{\sqrt{2}}\mathrm{sech}^2\left(\frac{z}{2z_c}\right), \tag{7.2}$$

$$V_2(z)=\frac{3}{2}\mathrm{sech}^2\left(\frac{z}{2z_c}\right).$$

The above solutions are particularly useful, as analytic forms of gap simultons can be constructed with them as the base. These can give us an insight into the physical processes involved, and allow soliton energies to be readily estimated. In cases with $\gamma\neq 1$, the solutions are given in numerical form. The corresponding band-gap simultons can be obtained using the mapping relationship, Eq. (7.1), with a numerical differentiation for its imaginary part.

Coupling 1: For example, for the case $\kappa_2>0$, $s_1=s_2=-1$ and $\gamma=1$ (coupling between lower branches), the gap simultons are obtained by substituting the above solutions into Eq. (7.1),

$$\vec{\mathcal{A}}_1=\frac{\pm 3a_1}{\sqrt{2}}\left(\mathrm{sech}^2\left(\frac{z}{2z_c}\right)\begin{bmatrix}\mathrm{sgn}(\kappa_1)\\ 1\end{bmatrix}+\frac{\mathrm{sech}^2\left(\frac{z}{2z_c}\right)\tanh\left(\frac{z}{2z_c}\right)}{2z_c|\kappa_1|}\begin{bmatrix}-\mathrm{sgn}(\kappa_1)i\\ i\end{bmatrix}\right),$$

$$\vec{\mathcal{A}}_2=\frac{-3a_2}{2}\left(\mathrm{sech}^2\left(\frac{z}{2z_c}\right)\begin{bmatrix}1\\ 1\end{bmatrix}+\frac{\mathrm{sech}^2\left(\frac{z}{2z_c}\right)\tanh\left(\frac{z}{2z_c}\right)}{2z_c|\kappa_2|}\begin{bmatrix}-i\\ i\end{bmatrix}\right). \tag{7.3}$$

Coupling 2: Similarly, solutions to the case $\kappa_2<0$, $s_1=s_2=1$ and $\gamma=1$ (coupling between upper branches) are given as

$$\vec{\mathcal{A}}_1=\frac{\pm 3a_1}{\sqrt{2}}\left(\mathrm{sech}^2\left(\frac{z}{2z_c}\right)\begin{bmatrix}\mathrm{sgn}(\kappa_1)\\ -1\end{bmatrix}+\frac{\mathrm{sech}^2\left(\frac{z}{2z_c}\right)\tanh\left(\frac{z}{2z_c}\right)}{2z_c|\kappa_1|}\begin{bmatrix}\mathrm{sgn}(\kappa_1)i\\ i\end{bmatrix}\right),$$

$$\vec{\mathcal{A}}_2=\frac{3a_2}{2}\left(\mathrm{sech}^2\left(\frac{z}{2z_c}\right)\begin{bmatrix}1\\ 1\end{bmatrix}+\frac{\mathrm{sech}^2\left(\frac{z}{2z_c}\right)\tanh\left(\frac{z}{2z_c}\right)}{2z_c|\kappa_2|}\begin{bmatrix}i\\ -i\end{bmatrix}\right). \tag{7.4}$$

For both cases, it is possible that $\mathrm{sgn}(\kappa_1)=-\mathrm{sgn}(\kappa_2)$, which means that both refractive index modulations are out of phase.

As a numerical example, we will show briefly that the pulse energy of a one-dimensional gap simulton is possibly of the order of pJ. We consider a waveguide made of $LiNbO_3$ and a laser whose free-space wavelength is $\lambda_1=1.06$ μm and whose pulse width is 10 ps. From Eq. (6.22), the pulse energy depends on the soliton volume through the volume factors in front of the integral, while the exact dimensionless soliton envelope is included in the integral. This depends on both the dimensionality and the factor γ in the equations themselves, and usually has to be evaluated numerically. We will choose the special case of $\gamma=1$, where the pulse envelopes have an analytic form.

We use the typical values $\chi^{(2)}=11.9$ pm/V [42] and the average refractive index of the waveguide, $\overline{n}=2.5$. We assume the refractive index modulation to be 0.2% of $\overline{n}$, at each wavelength, so that $\Delta_{jj}\simeq 0.002$. This gives coupling parameters of $\kappa_1\simeq 0.001\overline{k}=0.001\times 2\pi\overline{n}/\lambda_1=1.5\times 10^4$ m^{-1}, $\kappa_2\simeq 2\times\kappa_1$, and $\chi_E\simeq\overline{k}\chi^{(2)}/\overline{n^2}\simeq 3\times 10^{-5}$ V^{-1}. For a 10-ps pulse, we have $z_c\simeq 10^{-11}c/\overline{n}\simeq 1.2$ mm, where c is the speed of light in free space. This in turn gives the soliton period or reshaping time, $q^{-1}\simeq 350$ ps. The amplitude of a simulton is therefore of the order $q\overline{n}/(\chi_E c)\simeq 1.2\times 10^6$ V m^{-1}. Using the above values, we find that $W(z_c)\simeq 75$ J m^{-3}. Substituting $W(z_c)$ into Eq. (6.21), and assuming $\gamma=1$ and $\sigma=2$, we find the the combined pulse

energy is around 40 pJ for an effective waveguide area of 25 μm^2.

This pulse energy is many orders of magnitude lower than the usual values for the corresponding $\chi^{(3)}$ gap solitons. An inspection of Eq. (6.22) shows clearly that the energy density requirements are greatly reduced if κ and/or $\chi^{(2)}$ are increased, at fixed z_c. Thus, further reductions in pulse energy can be readily obtained if larger values of κ are used, together with shorter pulse lengths.

B. Exact one-dimensional solutions

One way of testing the validness of the EMA approach is to solve the classical equation directly using a numerical method. Without knowing the basic form of the gap simulton solutions, solving the parametric gap equation numerically based on the shooting method is difficult as the two boundary points are adjustable in a eight-dimensional phase space. However, if we assume that the propagating and antipropagating waves are complex conjugate ($\mathcal{A}_{j-}=\mathcal{A}_{j+}^*$ at $t=0$), the searching task can be reduced to be four-dimensional. Solutions to the parametric gap equations are written in the form

$$\mathcal{A}_{j\pm}(z,\tau)=\sqrt{\frac{j}{2}}\frac{1}{\chi_E}[p_j(z)\pm iq_j(z)]e^{-ij\alpha t},\quad j=1,2, \tag{7.5}$$

where $\alpha=s_1v_1\kappa_1-\delta k_1-q$. Although this ansatz is not in the most general form, it can still generate soliton solutions, as we will show.

Substituting the above ansatz into Eq. (2.12), and looking for stationary solutions, we have

$$\frac{dq_1}{dz}=K_{1+}p_1+p_1p_2+q_1q_2,$$

$$\frac{dp_1}{dz}=-K_{1-}q_1-p_1q_2+p_2q_1,$$

$$\frac{dq_2}{dz}=K_{2+}p_2+\frac{1}{2}(p_1^2-q_1^2),$$

$$\frac{dp_2}{dz}=-K_{2-}q_2-p_1q_1, \tag{7.6}$$

where $K_{j\pm}=j\alpha/v_j+\delta k_j\pm\kappa_j$, $j=1$ and 2.

Regarding z as the ''time,'' p_j as general momenta, and q_j as general coordinates, we derive the above equations from the Hamiltonian

$$H=\sum_{j=1}^{2}\left(\frac{K_{j+}}{2}p_j^2+\frac{K_{j-}}{2}q_j^2\right)+\frac{1}{2}(p_1^2-q_1^2)p_2+p_1q_1q_2. \tag{7.7}$$

The above equation can be visualized as the equation of motion of a virtual particle in a four-dimensional phase space. When time $z\to\pm\infty$ in the four-dimensional phase space, we have $(q_1,p_1,q_2,p_2)\to(0,0,0,0)$. When time $z\to 0$, $(q_1,p_1,q_2,p_2)\to(0,p_1,0,p_2)$. According to the topological argument [16], a soliton forms whenever the particle returns to its starting critical point. Therefore, the procedure of searching a soliton numerically is to place a virtual particle at point $(0,p_1,0,p_2)$, and adjust the values of p_1 and p_2 until it returns to $(0,0,0,0)$. We can further reduce the above two-dimensional searching process into a one-dimensional one. Noting the Hamiltonian H is a conserved quantity and $H=0$ at $(0,0,0,0)$, we conclude that $H=0$ also at $(0,p_1,0,p_2)$. This gives a relationship between p_1 and p_2,

$$p_1=\sqrt{\frac{-K_{2+}}{(K_{1+}+p_2)}}p_2. \tag{7.8}$$

Thus, with a correct value of p_2, a virtual particle returns to $(0,0,0,0)$, forming a gap simulton solution.

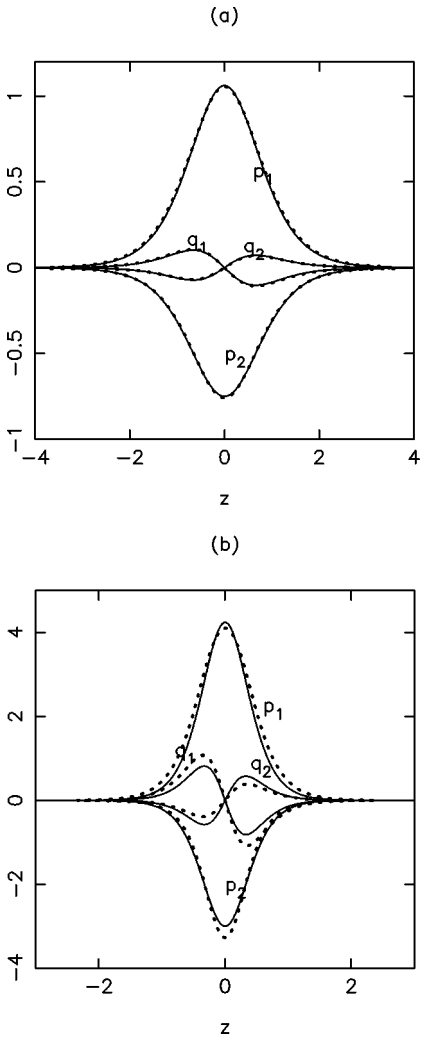

FIG. 3. Gap simultons obtained via direct numerical method (dotted lines) and EMA analytic analysis (solid lines). The dimensionless parameters used for simplicity were $\kappa_1=\kappa_2=4$, $\gamma=1$, $v_1=v_2=1$, $\delta k_1=0$, and $\chi_E=1$. (a) $z_c=\frac{1}{2}$, $\delta k_2=\frac{7}{2}$. (b) $z_c=\frac{1}{4}$, $\delta k_2=2$.

This numerical method gives an excellent agreement with the previous analytic analysis when the EMA approximation is valid. An example is shown in Fig. 3(a). Although $\kappa_j z_c=2$, which is not greatly larger than 1, the difference between the numerical solution and the analytical solution is negligible. The difference becomes noticeable only when $\kappa_j z_c=1$, but it is still small compared with the solution's

imaginary part. This is shown in Fig. 3(b). Such a small difference is unlikely to change a solution's stability dramatically unless the solution is along the boundary of stability.

Cases that involve cross couplings between the upper branch and the lower branch of different gaps result in dark simulton solutions. These are not available analytically, and therefore must be calculated numerically—as is also necessary for all nontopological cases with $\gamma \neq 1$. Obtaining a topological gap simulton is a relatively easy task based on the previous analysis. One solves the dispersive parametric equations numerically for topological simultons. The corresponding topological gap simultons can then be obtained using Eq. (7.1), involving a numerical differentiation for the imaginary part. In conclusion, the EMA provides a reliable and accurate method for solving the coupled band-gap equations, even when compared with a direct numerical method which gives exact solutions.

C. Higher-dimensional solutions

The dispersive parametric equations we obtain also support higher-dimensional soliton solutions [37,16] in $2+1$ and $3+1$ dimensions. These correspond to striped or layered band-gap structures, respectively. Equation (2.12), the one-dimensional coupled Maxwell equation, can be extended to two- or three-dimensional structures in the paraxial approximation, by adding a transverse Laplacian to each of the earlier propagation equations. The equations describing the propagation of higher-dimensional gap simultons are therefore written as

$$
\begin{aligned}
&i\left[\frac{1}{v_1}\frac{\partial}{\partial t}+\frac{\partial}{\partial z}\right]\mathcal{A}_{1+}+\frac{1}{2\bar{k}}\nabla^2\mathcal{A}_{1+}+\delta k_1\mathcal{A}_{1+}+\kappa_1\mathcal{A}_{1-}\\
&\quad+\chi_E\mathcal{A}_{1+}^{*}\mathcal{A}_{2+}=0,\\
&i\left[\frac{1}{v_1}\frac{\partial}{\partial t}-\frac{\partial}{\partial z}\right]\mathcal{A}_{1-}+\frac{1}{2\bar{k}}\nabla^2\mathcal{A}_{1-}+\delta k_1\mathcal{A}_{1-}+\kappa_1\mathcal{A}_{1+}\\
&\quad+\chi_E\mathcal{A}_{1-}^{*}\mathcal{A}_{2-}=0,\\
&i\left[\frac{1}{v_2}\frac{\partial}{\partial t}+\frac{\partial}{\partial z}\right]\mathcal{A}_{2+}+\frac{1}{4\bar{k}}\nabla^2\mathcal{A}_{2+}+\delta k_2\mathcal{A}_{2+}+\kappa_2\mathcal{A}_{2-}\\
&\quad+\chi_E\mathcal{A}_{1+}^{2}=0,\\
&i\left[\frac{1}{v_2}\frac{\partial}{\partial t}-\frac{\partial}{\partial z}\right]\mathcal{A}_{2-}+\frac{1}{4\bar{k}}\nabla^2\mathcal{A}_{2-}+\delta k_2\mathcal{A}_{2-}+\kappa_2\mathcal{A}_{2+}\\
&\quad+\chi_E\mathcal{A}_{1-}^{2}=0,
\end{aligned}
\tag{7.9}
$$

where $\nabla^2=\partial^2/\partial x^2$ for $2+1$ dimensions, and $\nabla^2=\partial^2/\partial x^2+\partial^2/\partial y^2$ for $3+1$ dimensions.

Using the Hamiltonian method to obtain equations in the EMA for this case once again results in much simpler equations. With the mapping relationship [Eq. (7.1)], we can transform the above equation approximately into the form of Eq. (6.11). This equation has also been analyzed previously, and it has been proved that an equation identical in form to Eq. (6.11) supports stable simultons in both two and three dimensions [38,39,21,37]. This indicates that the parametric band-gap environment is also able to support higher-dimensional solitons. Thus, it is possible to obtain parametric gap solitons in up to three spatial dimensions. If $\tilde{s}_2=1$, solutions are cylindrically symmetric, and can be obtained exactly using numerical technique [16]. Such a condition is not necessary satisfied, and nonsymmetric solutions can be obtained approximately via a variational method [21].

An unusual property of the higher-dimensional gap parametric solitons is that they provide an example of a nonlinear, three-dimensional self-confined object. These can even appear stationary in the laboratory frame. Of course, this raises the practical question of how an object of this type could be generated with external laser fields. Apart from inserting a gain medium into the Bragg grating, it is likely that a slightly detuned, and therefore moving, soliton would be more practical—since it could then be coupled through a spatial boundary of the nonlinear volume grating. Another practical consideration is the question of losses, which are neglected here. These are likely to be very significant for slowly moving gap solitons, due to the long interaction times with a possibly lossy environment.

As we have calculated previously for the one-dimensional gap simultons, the pulse energy of higher-dimensional gap simultons can be estimated similarly. Assuming the same nonlinear material and pulse width, we find that the energy density scaling coefficients are $W(z_c)\simeq 75$ J m^{-3} as before. We also find that $r_c\simeq 4\times 10^{-5}$ m. Substituting these values into Eq. (6.21) and assuming cylindrically symmetric solutions, we find that the pulse energy is around 2 nJ for the two-dimensional case ($\gamma=1$, and a width of waveguide $\simeq 5\mu$m), and around 55 nJ for the three-dimensional case ($\gamma=3$). A larger value of γ was chosen in the three-dimensional case, as this gives an improved stability. Note that exact phase matching implies that $\gamma=4$ [i.e., $\beta(s_1,s_2)=0$], and this is also stable. In these cases, the dimensionless integrals were carried out numerically, using the shooting technique [16] to obtain the pulse envelopes. Another posibility is to use a variational method [21], which allows the integrals to be evaluated analytically to a good approximation.

The total energy for $D>1$ depends strongly on the radial parameter r_c, which scales as $z_c\sqrt{\kappa}$ at a fixed wavelength. This means that the aspect ratio of the pulse changes as κ increases, which increases the ratio of radius to length—changing the soliton from an elongated ''cigar'' at small κ, to a more spheroidal shape at large κ. Despite this, it is still favorable to increase κ, if a lower pulse energy is required at a given pulse length z_c. To reduce the pulse length and pulse energy simultaneously, it is most favorable to fix the product of $z_c\sqrt{\kappa}$—which determines the radius—while reducing z_c and increasing κ, until the EMA limit of $\kappa z_c\simeq 1$ is nearly reached. Note that a given value of the product $z_c\sqrt{\kappa}$ determines both the corresponding energy density factor *and* the radius scale in higher dimensions; these are modified, of course, by the solutions to the corresponding dimensionless equations.

VIII. STABILITY

The important question of the stability of the parametric band-gap simultons is investigated here by numerically solv-

ing the original band-gap equations (2.12), using the effective-mass approximation solution from the Hamiltonian method as an initial condition. The numerical simulation is based on the implicit central-difference (split-step) Fourier-transform scheme [40]. While the simplified equations are known to be stable, these are not exact equations for the gap-soliton problem. Thus, there are possible additional instabilities that may arise from invalidation of the EMA, group-velocity mismatch effects, or other internal properties of the band-gap simultons. This investigation does not address the issue of whether the paraxial and slowly varying envelope approximations are themselves always applicable here.

To provide a suitable perturbation, the (small) imaginary part of the input solution was usually omitted. If the imaginary part is included, a steady propagation of gap simultons is observed when the simulton is stable, and even an unstable solution can survive in a metastable fashion for a relatively long time. By omitting this, the initial condition is observed to either evolve toward a stable wave, or to rapidly decay. Unless stated otherwise, the inputs used were obtained from the simplified EMA analysis, which in most cases gives an excellent approximate starting profile. An exception to this was the test of stability at small z_c, where we cannot expect the EMA to be even approximately valid. In these cases, we used the exact one-dimensional initial solutions described in Sec. VII, with the imaginary part included.

For simplicity, Eq. (2.12) is treated as if it were a dimensionless equation in all of our simulations. The nonlinear coefficient χ_E is usually taken as 1, and the phase mismatch of the fundamental harmonic is taken as 0. In the one-dimensional cases when $\gamma=1$, the analytical form [Eqs. (7.3) or (7.4)] is used. Otherwise, numerical solutions transformed from solutions in Ref. [16] are used. The transverse lattice size is normally 1024 for one dimension, 64×64 for two dimensions, and $40\times40\times40$ for three dimensions. The propagation step size is chosen such that the local error is less than 1%, by comparing results at two different time steps.

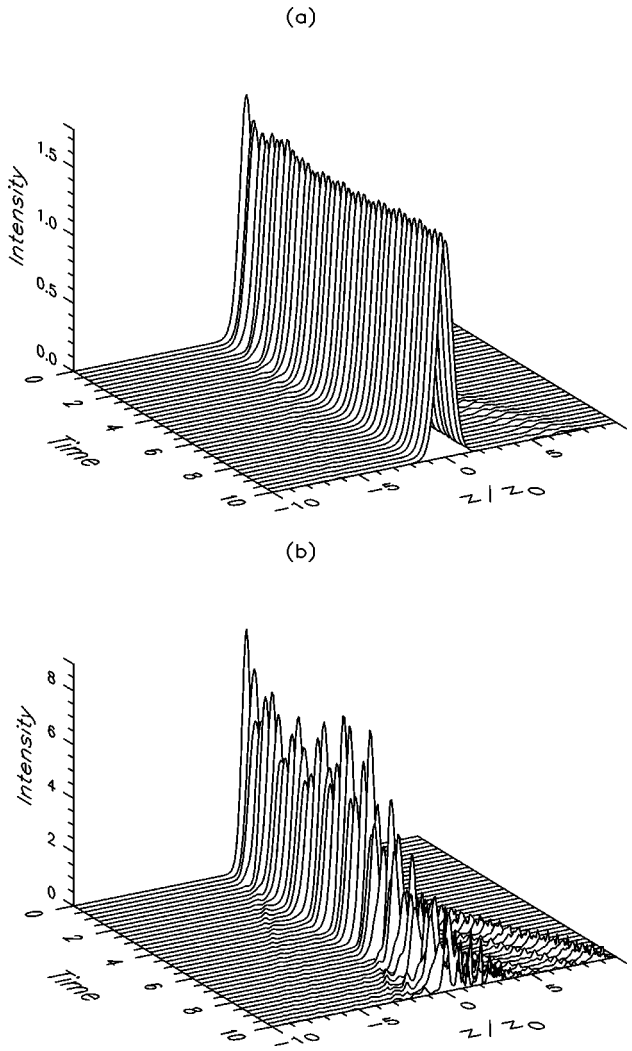

FIG. 4. Instability when the EMA is invalid. Only the fundamental harmonic is shown. (a) Quasistable simulton when $z_c\kappa_1=1.5$. (b) Unstable simulton when $z_c\kappa_1=1$. The dimensionless parameters used for simplicity were $\chi_E=1$, $\kappa_1=\kappa_2=4$, $\gamma=1$, $v_1=v_2=1$, and $\delta k_1=0$. (a) $z_c=\frac{3}{8}$, $\delta k_2=\frac{28}{9}$. (b) $z_c=\frac{1}{4}$, $\delta k_2=2$.

A. EMA and stability

The condition that the EMA is valid can be understood as $z_c\kappa_j\gg1$. In order to investigate possible instabilities when the EMA is invalid, we reduce the value of z_c while fixing the values of κ_j. We find that gap simultons become unstable when $z_c\kappa_j\approx1$. In order to verify the existence of the instability, an exact numerical solution of the full coupled gap equations (including the imaginary part of the solution) was also used. Unstable propagation was observed for all cases when $z_c\kappa_j<1$.

Two such cases are shown in Fig. 4. Simultons appear to be stable even when $\kappa_1 z_c=1.5$, as illustrated in Fig. 4(a). When $\kappa_1 z_c=1$, we see an unstable gap simulton [Fig. 4(b)]. In these graphs, the value of γ was 1, and the analytical solution, Eq. (7.3), was used without the imaginary part.

These results show that the EMA, which was introduced here as a useful approximation to simplify the equations, also in a sense delineates the physical region where stable solutions can be expected to occur. If the fields have frequency components which extend well outside the band-gap region, the EMA is of course invalid. In addition to this, the corresponding solitons rapidly become unstable, even if all the calculations are carried out without appealing to the EMA. Thus the useful region of this approximation also appears to correspond to the region of most physical interest for soliton formation, which provides a justification for the use of this method.

This does not exclude the possibility that some exotic solutions exist when the EMA is invalid. For example, it is possible that there could be solutions which do not occur in the EMA limit, due to symmetry considerations outlined previously, but which are stable in some transition region where there are frequency components near the edges of the band gap. We have not investigated novel solutions of this type.

B. Material group-velocity mismatch

In a real experiment, the first harmonic and the second harmonic usually have different material group velocity. Does such a group-velocity mismatch introduce a new instability?

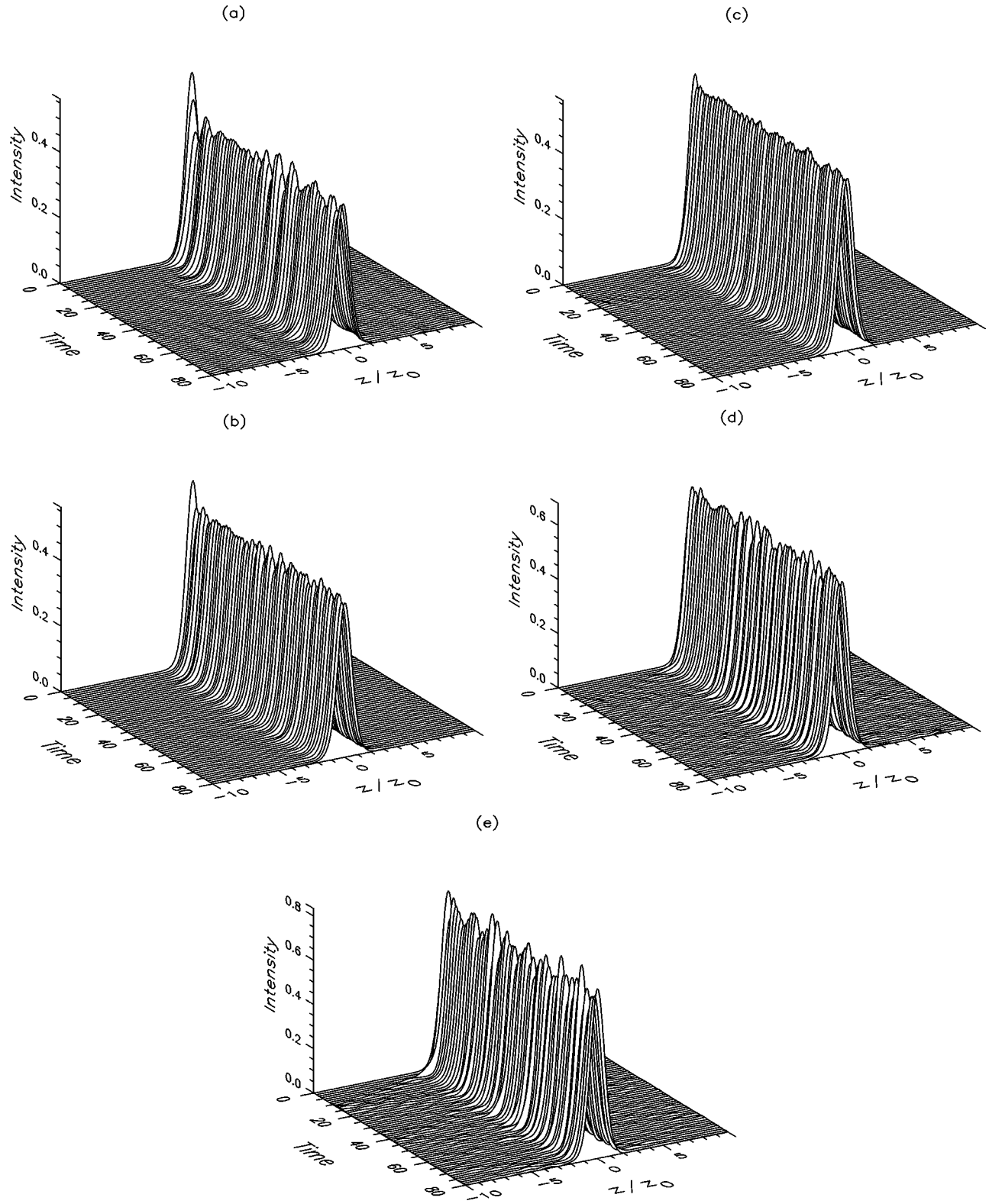

FIG. 5. Stable propagation of gap simultons with significant material group velocity mismatch. Only the fundamental harmonic is shown. The dimensionless parameters used were $\delta k_1=0$, $\kappa_1=\kappa_2=4$, $\chi_E=1$, $\gamma=1$, $v_2=1$, and $z_c=\frac{1}{2}$. (a) $v_1=0.5$, $\delta k_2=-0.25$. (b) $v_1=0.75$, $\delta k_2=1.625$. (c) $v_1=1.0$, $\delta k_2=3.5$ (group velocity matched case). (d) $v_1=1.5$, $\delta k_2=7.25$. (e) $v_1=2.0$, $\delta k_2=11.0$.

We have performed a series of numerical simulations in a one-dimensional band-gap environment to answer this question. We first fixed the material group velocity of the second harmonic and then adjusted the material group velocity of the first harmonic so that the ratio (v_1/v_2) varied from 0.5 to 2 with a step size of 0.25. Stable propagation was observed for all cases even under extreme circumstances, such as $v_1/v_2=0.5$ and 2, although oscillations did occur when the departure of the ratio away from one was more than 0.5. Similar results have also been obtained on varying the veloc-

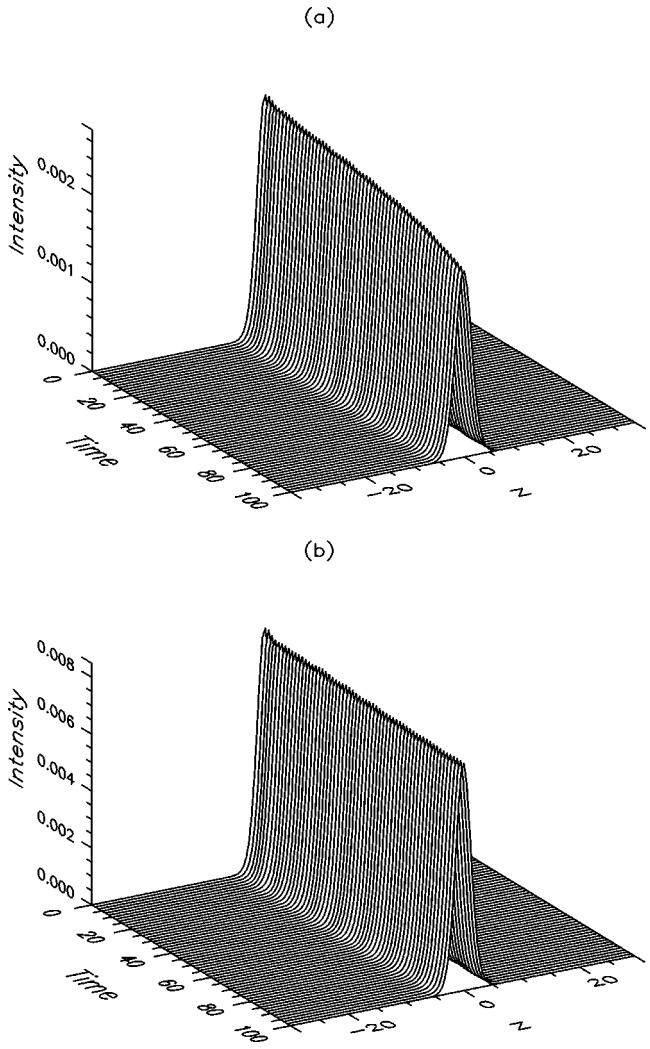

FIG. 6. Transition of stability of gap simultons. Only the fundamental harmonic is shown. The dimensionless parameters used were $\delta k_1=0$, $\kappa_1=\kappa_2=4$, $v_1=v_2=1$, $\chi_E=1$, and $z_c=1$. (a) Decaying propagation: $\gamma=0.05, \delta k_2=3.756\,25$. (b) Stable propagation: $\gamma=0.2, \delta k_2=3.775$.

ity of the second harmonic while fixing that of the first harmonic. This result is particularly encouraging for experiments, since gap simultons can form within a wide range of material group-velocity mismatch, thus avoiding the difficult task of matching group velocities.

A set of simulations demonstrating stable propagation of band-gap simultons is shown in Fig. 5. We used $\kappa_1=\kappa_2=4.0$, $z_c=0.5$, and $v_2=1.0$ for all cases. The value of v_1 increases from 0.5 to 2.0 by an interval of 0.25.

C. Internal stability of the band-gap simultons

The stability of conventional simultons is a function of two parameters, the ratio between dispersion and the phase mismatch [41]. Similarly, we expect that the stability of gap simultons is also (at least partially) determined by $\sigma=v_1\kappa_2/(v_2\kappa_1)$ and γ. Generally, a simulton solution of Eq. (6.5) becomes unstable for large σ and small γ. For example, a one-dimensional simulton becomes unstable when $\gamma<0.1$ for $\sigma=1$.

It is likely that a similar instability also exists in the band-gap system. In order to test this, we have performed a series

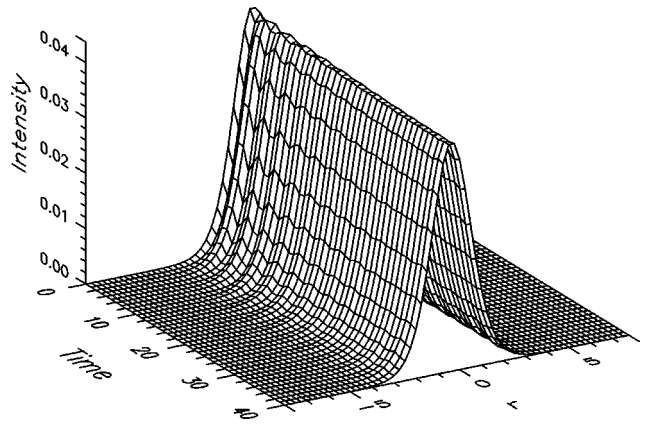

FIG. 7. Stable propagation of a (2+1)-dimensional gap simulton. Only the fundamental harmonic is shown. Initial conditions were cylindrically symmetric in the reduced (EMA) coordinate system. The dimensionless parameters used for simplicity were $q=1/8$, $-\kappa_2=2\kappa_1=8$, $z_c=1$, $\gamma=1$, $v_1=v_2=1$, $\delta k_1=0$, $\delta k_2=\frac{3}{16}$ and $\chi_E=1$.

of simulations for $\sigma=1$. In these simulations, we vary the value of γ so that $\gamma=0.05$, 0.1, 0.2, and 0.3. Unstable band-gap simultons have been observed for $\gamma=0.05$ and 0.1.

The stability transition is shown in Fig. 6. Two plots of simulton propagation are given. Figure 6(a) depicts a band-gap simulton decaying for $\gamma=0.05$ and $\sigma=1.0$. Figure 6(b) is a steady propagation of a band-gap simulton with $\gamma=0.2$ and $\sigma=1.0$. These simulations demonstrate, as expected, that the simplified EMA equations and their known stability properties are an accurate representation of the stability properties of the full coupled equations under the conditions of applicability of the EMA. Most importantly, it appears that there are no new internal instabilities, at least in the one-dimensional cases treated here.

D. Higher-dimensional stability

Using the mapping relationship [Eq. (7.1)], we obtained higher-dimensional band-gap simultons from known higher-dimensional conventional parametric simultons. Although nonsymmetric solutions (in different spatial directions) are possible, here we only show solutions obtained under circumstances where the simplified dimensionless EMA equations are rotationally symmetric. Under these conditions, appropriate initial conditions are obtained by solving the simplified equations exactly via the numerical shooting technique [16], based on the EMA equations.

In the case of the propagation equations that are applicable in the EMA limit, there is a number of results available on stability in two and three dimensions [38,39,21,37]. In particular, it is known that no self-focusing collapse is possible. Stable propagation is expected from a Lyapunov [38,39] analysis, for all cases with $\delta=1$, $\sigma=2$, and $\beta<0$, which corresponds to $\gamma>4$ in our dimensionless notation. Here we only consider couplings near the upper band gap (i.e., $s_1=s_2=1$). A variational and numerical treatment [21] indicates that an even wider stability region is possible, although not extending as far as $\gamma=0$ in any case.

After obtaining appropriate initial estimated solitons, they are propagated numerically using the four coupled partial

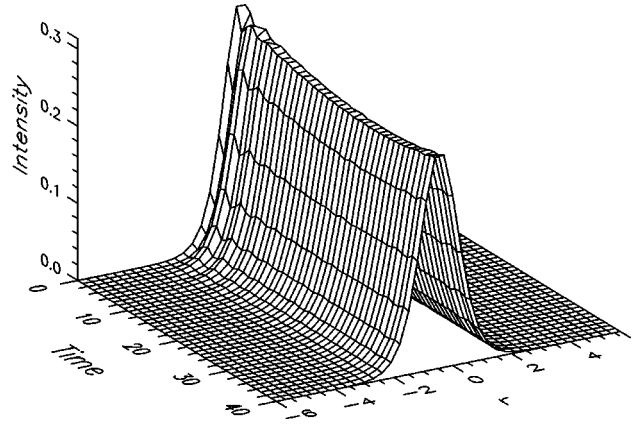

FIG. 8. Stable propagation of a (3+1)-dimensional gap simulton. Only the fundamental harmonic is shown. Initial conditions were cylindrically symmetric in the reduced (EMA) coordinate system. The dimensionless parameters, used for simplicity, were $q=\frac{1}{8}$, $-\kappa_2=2\kappa_1=8$, $z_c=1$, $\gamma=3$, $v_1=v_2=1$, $\delta k_1=0$, $\delta k_2=\frac{1}{16}$, and $\chi_E=1$.

differential equations, as before. Our results in Fig. 7 show a (2+1)-dimensional gap simulton propagation, with the complete set of equations. After a small initial oscillation, the gap simulton reaches a steady state, proving the stability of the soliton in two dimensions, with values of $\gamma=1$, $\delta=1$, and $\sigma=2$. Variational initial conditions [21] have been investigated elsewhere, indicating that stable propagation should occur for (at least) $\gamma\geqslant 0.7$ with these values of δ and σ.

Similar results in Fig. 8 show a (3+1)-dimensional gap simulton propagation, with the complete set of equations, and parameters corresponding to $\gamma=3$, $\delta=1$, and $\sigma=2$. No assumption of radial symmetry was used in solving these equations, which were treated on a full four-dimensional space-time lattice. The gap simulton also reaches a steady state after a small initial oscillation. This indicates that we can have stable (3+1)-dimensional gap simultons, at least with $\gamma=3$. While the general stability in this case is poorly understood as yet, we note that the reduced propagation equations (without a band gap) are known [38,39] to have absolute stability for the case of perfect phase matching and above ($\gamma\geqslant 4$). We conjecture that there is stability for (at least) $\gamma\geqslant 3$, given an appropriate initial pulse energy.

IX. CONCLUSIONS

Using a coupled mode theory, we have obtained the classical band-gap equations describing a nonlinear parametric waveguide containing a volume Bragg grating. Without any further physical insight, these equations are difficult to analyze for simultaneous solitary wave solutions or simultons, due to their high phase space dimension. We therefore developed a Hamiltonian theory which treats one-, two-, and three-dimensional propagation of eigenmodes of the linear equations, instead of plane waves. Using the effective-mass approximation, we obtained a pair of coupled equations which are formally identical to the coupled equations describing a conventional dispersive parametric medium. The solutions found this way are stable, multidimensional solitons—provided the pulse itself is tuned to the upper edge of the band gap, and satisfies the restriction that $\kappa z_c>1$. This physically means just that the Fourier components of the pulse are themselves mostly within the band gap.

A mapping relationship between the solutions of the approximate coupled equations and the solutions of the classical band-gap equations was established. This mapping relationship helps to reduce the number of phase space dimensions, and makes analytical solutions possible in special cases. The approximations used in obtaining the mapping relationship are well justified, since the EMA solutions agree with exact numerical solutions, under the stated conditions for applicability of the approximation. Direct numerical simulation of the complete classical band-gap equation show steady propagation of simultons, using the EMA solutions as the initial condition, provided the pulse bandwidth is small compared to the width of the band gap in frequency space. Additional restrictions on the phase mismatch are also necessary, although we find that group velocity matching is only important for solitons moving in the laboratory frame.

In summary, a parametric band-gap waveguide can provide both large dispersion and large nonlinearity. An experimentally relevant point is that the solutions given already are mostly completely stationary in the laboratory frame. This creates an unexpected problem: how can they be introduced into the band-gap material? In fact, this is easily solved. If the gap structure is fabricated with $m_2=2m_1$, there is a symmetry in the equations which allows for moving solutions with an identical form to the stationary ones. Thus they can be generated at the boundary, and then move longitudinally into the bulk medium. If there is group-velocity matching, it is also possible to have transversely moving solutions—which creates yet another possible means of introducing the soliton into the band-gap medium.

We have not treated the problems of boundary interactions here. It should be noted that perturbations may arise which could limit the lifetime of the solitons, owing to processes omitted in the original equations. These include material losses (absorption), as well as Raman scattering, four-wave mixing, and any diffractive effects which are omitted from the paraxial approximation. Nevertheless, it is clearly physically interesting that at least a quasistable type of solitary wave can be generated in two or three dimensions. Most, if not all previous studies of physically relevant soliton equations were restricted to just one spatial dimension. This restriction is clearly unnecessary, although the price that is paid is the use of equations defined in a higher-dimensional phase space, which do not satisfy classical integrability requirements.

The two- and three-dimensional simultons may have potential applications to all-optical signal processing, including high-speed switching [43], frequency shifting, pulse shaping, multiplexing, demultiplexing, and signal replication. There are possible advantages over other soliton-based optical switches, due to the short interaction distances, low power requirements, and interesting stability properties of the gap simulton. In particular, stability in higher dimensions means that information can be encoded in the signal propagation direction, which could help in distinguishing different input and output signals in a logic gate. Response times are only limited by the electronic response of the nonlinear medium, which typically occurs over femtosecond time scales. Para-

metric band-gap devices can be fabricated in compact sizes [44], with fast response times, and using power levels similar to those in communication systems.

These characteristics of fast interaction times, low pulse energy, and stability in higher dimensions make the gap parametric system an ideal soliton environment for both fundamental physics and applications of solitons.

ACKNOWLEDGMENTS

The authors are grateful for the support of the Australian Research Council. The authors also wish to thank Dr. B. A. Malomed and Dr. Martijn de Sterke for useful discussions. This research was supported in part by the National Science Foundation under Grant No. PHY94-07194.

[1] Y. N. Karamzin and A. P. Sukhorukov, Moscow Univ. Phys. Bull. **20**, 339 (1974).
[2] Y. N. Karamzin and A. P. Sukhorukov Zh. Éksp. Teor. Fiz. **68**, 834 (1975) [Sov. Phys. JETP **41**, 414 (1976)].
[3] G. Valiulis and K. Staliunas, Lith. Phys. J. **31**, 61 (1991).
[4] M. J. Werner and P. D. Drummond, J. Opt. Soc. Am. B **12**, 2390 (1993).
[5] M. J. Werner and P. D. Drummond, J. Opt. Soc. Am. B **10**, 2390 (1993).
[6] R. Schiek, J. Opt. Soc. Am. B **10**, 1848 (1993).
[7] M. J. Werner and P. D. Drummond, Opt. Lett. **19**, 613 (1994).
[8] M. A. Karpierz and M. Sypek, Opt. Commun. **110**, 75 (1994).
[9] C. R. Menyuk, R. Schiek, and L. Torner, J. Opt. Soc. Am. B **11**, 2434 (1994).
[10] K. Hayata and M. Koshiba, Phys. Rev. A **50**, 675 (1994).
[11] A. V. Buryak and Y. S. Kivshar, Opt. Lett. **19**, 1612 (1994).
[12] L. Torner, C. R. Menyuk, and G. I. Stegeman, J. Opt. Soc. Am. B **12**, 889 (1995).
[13] L. Torner, Opt. Commun. **114**, 136 (1995).
[14] L. Torner, C. R. Menyuk, and G. I. Stegeman, Opt. Lett. **19**, 1615 (1994).
[15] A. V. Buryak and Y. S. Kivshar, Phys. Rev. A **51**, R41 (1995).
[16] H. He, M. Werner, and P. D. Drummond, Phys. Rev. E **54**, 896 (1996).
[17] A. V. Buryak and Y. S. Kivshar, Opt. Lett. **20**, 834 (1995).
[18] A. V. Buryak, Y. S. Kivshar, and V. V. Steblina, Phys. Rev. A **52**, 1670 (1995).
[19] A. V. Buryak and Y. S. Kivshar, Phys. Lett. A **197**, 407 (1995).
[20] W. E. Torruellas *et al.*, Phys. Rev. Lett. **74**, 5036 (1995).
[21] B. A. Malomed *et al.*, Phys. Rev. E **56**, 4725 (1997).
[22] B. J. Eggleton *et al.*, Electron. Lett. **32**, 1610 (1996).
[23] B. J. Eggleton *et al.*, Phys. Rev. Lett. **76**, 1627 (1996).
[24] C. M. de Sterke and J. E. Sipe, Prog. Opt. **XXXIII**, 203 (1994).
[25] H. He and P. D. Drummond, Phys. Rev. Lett. **78**, 4311 (1997).
[26] T. Peschel, U. Peschel, F. Lederer, and B. A. Malomed, Phys. Rev. E **55**, 4730 (1997).
[27] C. Conti, S. Trillo, and G. Assanto, Phys. Rev. Lett. **78**, 2341 (1997).
[28] T. D. Lee, *Particle Physics and Introduction to Field Theory*, revised and updated 1st ed. (Harwood, Chur, Switzerland, 1988), Vol. 1.
[29] M. Hillery and L. D. Mlodinow, Phys. Rev. A **30**, 1860 (1984).
[30] P. D. Drummond and S. J. Carter, J. Opt. Soc. Am. B **4**, 1565 (1987).
[31] P. D. Drummond, Phys. Rev. A **42**, 6845 (1990).
[32] M. G. Raymer, P. D. Drummond, and S. Carter, Opt. Lett. **16**, 1189 (1991).
[33] P. D. Drummond, Adv. Chem. Phys. **85**, 379 (1994).
[34] K. J. Ebeling, *Integrated Opto-electronics*, English ed. (Springer-Verlag, Berlin, 1992).
[35] A. Yariv and P. Yeh, *Optical Waves in Crystals* (Wiley, New York, 1984), Chap. 6.
[36] P. D. Drummond and H. He, Phys. Rev. A **56**, R1107 (1997).
[37] G. D. Boyd *et al.*, Appl. Phys. Lett. **5**, 234 (1964).
[38] K. Hayata and M. Koshiba, Phys. Rev. Lett. **71**, 3275 (1993).
[39] A. A. Kanashov and A. Rubenchik, Physica D **4**, 122 (1981).
[40] L. Bergé, V. K. Mezentsev, J. J. Rasmussen, and J. Wyller, Phys. Rev. A **52**, R28 (1995).
[41] P. D. Drummond, Comput. Phys. Commun. **29**, 211 (1983).
[42] D. E. Pelinovsky, A. V. Buryak, and Y. S. Kivshar, Phys. Rev. Lett. **75**, 591 (1995).
[43] P. D. Drummond, Opt. Commun. **49**, 219 (1984); M. N. Islam and C. E. Soccolich, Opt. Lett. **16**, 1490 (1991).
[44] E. M. Dianov, V. P. Konyaev, Yu. V. Kurnyavko, Sov. J. Quantum Electron. **21**, 360 (1991); W. P. Risk and S. D. Lau, Opt. Lett. **18**, 272 (1993).